TECHNISCHE UNIVERSITÄT WIEN
Vienna University of Technology

INSTITUT FÜR MECHANIK UND MECHATRONIK
Mechanics & Mechatronics

Diplomarbeit

# A novel approach to combine short- and long-term forecasts for energy management of heavy-duty fuel cell vehicles

ausgeführt zum Zwecke der Erlangung des akademischen Grades eines Diplom-Ingenieurs
unter der Leitung von

Associate Prof. Dipl.-Ing. Dr.techn. Christoph Hametner
Institut für Mechanik und Mechatronik
Abteilung für Regelungstechnik und Prozessautomatisierung

eingereicht an der Technischen Universität Wien

**Fakultät für Maschinenwesen und Betriebswissenschaften**

von

Matteas Jelovic
Matr.Nr.: 01425621

Wien, am 30. Mai 2022

Matteas Jelovic

# Eidesstattliche Erklärung

Ich erkläre eidesstattlich, dass ich die Arbeit selbständig angefertigt, keine anderen als die angegebenen Hilfsmittel benutzt und alle, aus ungedruckten Quellen, gedruckter Literatur oder aus dem Internet, im Wortlaut oder im wesentlichen Inhalt übernommenen Formulierungen und Konzepte, gemäß den Richtlinien wissenschaftlicher Arbeiten zitiert, durch Fußnoten gekennzeichnet bzw. mit genauer Quellenangabe kenntlich gemacht habe.

Wien, am 30. Mai 2022 Matteas Jelovic

# Danksagung

An dieser Stelle möchte ich besonders beim Herrn Associate Prof. Dipl.-Ing. Dr.techn. Christoph Hametner für die intensive Betreuung meiner Diplomarbeit bedanken. Die zahlreichen von uns geführten Gespräche, in denen wir Probleme und Lösungsansätze diskutiert haben, haben mir sehr viel Freude bereitet und mich stets für die Arbeit motiviert.
Mein Dank gilt auch dem Herrn Univ.Ass. Dott.mag. Alessandro Ferrara, der mir bei inhaltlichen und wissenschaftlichen Belangen stets ein Ansprechspartner war. Bei der gemeinsamen Teilnahme am 'VTS Motor Vehicles Challenge 2022' Wettbewerb hatte ich die Möglichkeit mich außerhalb meiner Diplomarbeit im Bereich Energiemanagement für Hybridfahrzeuge zu vertiefen. Das Ausarbeiten einer gewinnbringenden Strategie und die damit verbundenen Diskussionen werden mir immer positiv in Erinnerung bleiben.
Vielen lieben Dank auch an meine Mitstudierenden und allen Personen aus der Fachschaft, die für besonders viel Spaß und Motivation im Studium gesorgt haben.
Dankbar bin ich besonders meiner Freundin Lisa, für ihre hilfreiche Unterstützung, das entgegengebrachte Verständnis und ihren aufbauenden Worte während meines gesamten Studiums.
Abschließend möchte ich mich bei meinen Eltern bedanken, dir mir meine akademische Laufbahn ermöglicht und mich in all meinen Entscheidungen unterstützt haben. Aufgrund eurer unglaublichen Unterstützung konnte ich mich auf meine Interessen fokussieren und sorgenfrei studieren.

Diese Arbeit ist in Dankbarkeit meinen Eltern gewidmet.

# Kurzfassung

Der weltweite Energieverbrauch des Verkehrssektors nimmt aufgrund der Globalisierung ständig zu. Es wird zunehmend an alternativen Antriebssystemen geforscht, um die Umweltauswirkungen von schweren Nutzfahrzeugen zu verringern. In diesem Zusammenhang sind Brennstoffzellen-Elektrofahrzeuge eine der vielversprechendsten Lösungen zur Reduzierung der Treibhausgasemissionen. Diese Fahrzeugarchitektur umfasst ein Brennstoffzellensystem, das Wasserstoff in Elektrizität umwandelt - wobei nur Wasser als Nebenprodukt anfällt - und ein Batteriesystem, das die für Automobilanwendungen typischen schnellen Lastwechseln bewältigt. Daher ist eine Energiemanagementstrategie (EMS) erforderlich, um den elektrischen Leistungsbedarf zwischen den Brennstoffzellen-Batteriesystemen zu verteilen. Die Regelung der Leistungsaufteilung kann als komplexes Optimierungsproblem formuliert werden, das mehrere gegensätzliche Ziele beinhaltet, wie z. B. den Kraftstoffverbrauch, die Kontrolle des Ladezustands der Batterie und den Ampere-Durchsatz der Batterie. Mit Hilfe einer prädiktiven Energiemanagementstrategie kann die Leistungsaufteilung auf der Grundlage des künftigen Leistungsbedarfs optimiert werden, der anhand von Fahrdatenprognosen (z. B. Fahrzeuggeschwindigkeit, Streckenhöhe, Verkehrsstaus, Wetter) geschätzt wird. Die Fahrprognosen können je nach Länge des Prädiktionshorizonts in Kurzzeit- und Langzeitprognosen unterteilt werden, z. B. ein Horizont von einer Minute bzw. einer Stunde. Obwohl die Rechenkapazitäten industrieller Steuerungen stetig zunehmen, stellt die Online-Verarbeitung verschiedener langfristiger Vorhersageinformationen immer noch eine große Belastung für moderne Hardware dar. Unter der Annahme, dass beide Vorhersageebenen verfügbar sind, ist es daher interessant, neue Ansätze zu untersuchen, um die hohe Rechenkomplexität prädiktiver Regler zu bewältigen. In dieser Arbeit wird eine neuartige Formulierung für Model Predictive Control (MPC) vorgeschlagen, um eine prädiktive Energiemanagementstrategie mit langen Vorhersagehorizonten und wenigen Entscheidungsvariablen zu ermöglichen. Insbesondere wird die klassische MPC-Formulierung dahingehend modifiziert, dass sie nicht gleichmäßig verteilte Kontrollvariablen aufweist. Dadurch kann der prädiktive Regler kurzfristige Informationen (z.B. Verkehr) und langfristige Informationen (z.B. Streckenhöhe) berücksichtigen. Die vorgeschlagene Vorhersagestrategie wird anhand von realen Fahrzyklusdaten eines Straßengüterfahrzeuges getestet. Es wer-

den verschiedene Parameteränderungen und Prognoseszenarien angenommen, um die Wirksamkeit und Robustheit des MPC zu untersuchen. Die Ergebnisse zeigen, dass das vorgeschlagene Konzept optimale Kraftstoffverbrauchsergebnisse erzielt, Batterieladezustandskontrolle ermöglicht und gleichzeitig die Berechnungskomplexität eines MPC reduziert.

# Abstract

The world energy consumption of the transport sector is in constant growth due to globalisation. Increasing research is conducted on alternative propulsion systems to reduce the environmental impact of heavy-duty vehicles. In this context, fuel cell electric vehicles are one of the most promising solutions to reduce greenhouse gas emissions. This vehicle architecture includes a fuel cell system that converts hydrogen into electricity - with only water as a by-product - and a battery system that copes with the fast load transients typical of automotive applications. Therefore, an energy management strategy (EMS) is necessary to distribute the electric load demand between the fuel cell battery systems, usually referred to as the power-split control task. From a control theory point of view, the power-split task can be formulated as a complex optimisation problem involving several contrasting objectives, such as fuel consumption, battery state-of-charge (SoC) control, and battery ampere throughput. Using a predictive energy management strategy (PEMS), the power-split can be optimised based on the future load demand, estimated using driving information forecasts (e.g. vehicle speed, route elevation, traffic congestion level, weather). The driving forecasts can be classified into short-term and long-term, depending on the future horizon length, e.g. one minute ahead and one hour, respectively. Although computational capabilities of industrial controllers are steadily increasing, online processing of various long-term predictive information still places a heavy burden on modern hardware. Therefore, assuming that both forecast levels are available, it is interesting to investigate new approaches to deal with the high computational complexity of predictive controllers. This thesis proposes a novel model predictive control (MPC) formulation as a PEMS with long prediction horizons but few decision variables. In particular, the classical MPC formulation is modified to have non-uniformly distributed control variables. The PEMS can consider short-term information (e.g. traffic) and long-term information (e.g. route elevation). The proposed predictive strategy is tested on real-world driving cycles of road freight vehicles. Several parameter changes and forecast scenarios are adopted to examine the efficacy and robustness of the MPC. The results show that the proposed concept achieves optimal fuel consumption and SoC control results while reducing the computational complexity of MPC.

# Contents

# Chapter 1

# Introduction

## 1.1 Motivation

The switch to renewable energy sources is probably one of the most significant challenges of our time. Coal, oil and natural gas will become scarce in the near future, but also climate change is forcing us to reduce our consumption of fossil fuels significantly. Regulations and funding of governments stimulated the production of electric vehicles for the passenger car market worldwide. For the European Union, the share of electric vehicle registrations tripled from 3.5% in 2019 to over 11% in 2020 [1]. Due to heavy-load and range requirements, decarbonisation via electrification is not suitable for heavy-duty vehicles. They are responsible for about a quarter of $CO_2$ emissions from road transport in the European Union. In addition, road freight transport is expected to increase by 33% until 2030 and by 55% until 2050 [2].
Fuel cell electric vehicles (FCEV) can reduce the environmental impact and the dependence on fossil fuels. FCEVs use electricity, which is produced by a fuel cell system, to power an electric motor. Combined with a battery, such a mix of energy sources achieves a higher driving range, meets the fast power variations, and absorbs regenerative energy during brakes.
An energy management strategy (EMS) operates the power-split of the demanded power from the driver between multiple power sources (e.g. fuel cell, battery, supercapacitor) based on component constraints and efficiency criteria. The main objectives considered by an EMS are fuel economy, fuel cell lifetime, and battery lifetime [3]. These objectives include contrasting targets, such as hydrogen consumption, electric consumption, battery state-of-charge (SoC) control, and fuel cell voltage degradation minimisation. The SoC control target - essential to avoid accelerated degradation - is particularly challenging for trucks driving on hilly routes due to the heavy loads. An effective way to ensure that the battery charge stays within the desired operating range is to use a predictive energy management strategy (PEMS). With knowledge of the road gra-

dient, a PEMS can ensure that before an uphill section, the battery of an FCEV is fully charged to discharge it to the top of the hill so that energy can be regenerated by recuperation during the downhill drive. A non-predictive battery SoC control strategy will have suboptimal fuel economy during mountain routes.
The performance of a PEMS depends on the accuracy of prediction results of future driving conditions. A weather forecast for the next hour is a sufficiently long horizon, while a prediction of driver's behaviours is highly accurate only a few minutes ahead. Driving forecasts are classified into short-term and long-term information depending on the future horizon length. This thesis proposes a PEMS that processes short-term information (e.g. traffic) and long-term information (e.g. power demand). The architecture of the PEMS is shown in Figure 1.1. With the forecast of route speed and elevation from a navigation system, the long-term required electric power of the FCEV is predicted. Driving uncertainties (e.g., traffic, weather) influence drivers' behaviour. The resulting short-term information - speed and demanded electrical power - are used by the online PEMS to modify the predicted electric power and calculate the optimal fuel cell power. The adjustment of long-term predictive information with short-term information is repeated every step. This approach allows the PEMS to have a long-term insight into the future power demand while considering uncertainties like abrupt speed changes.

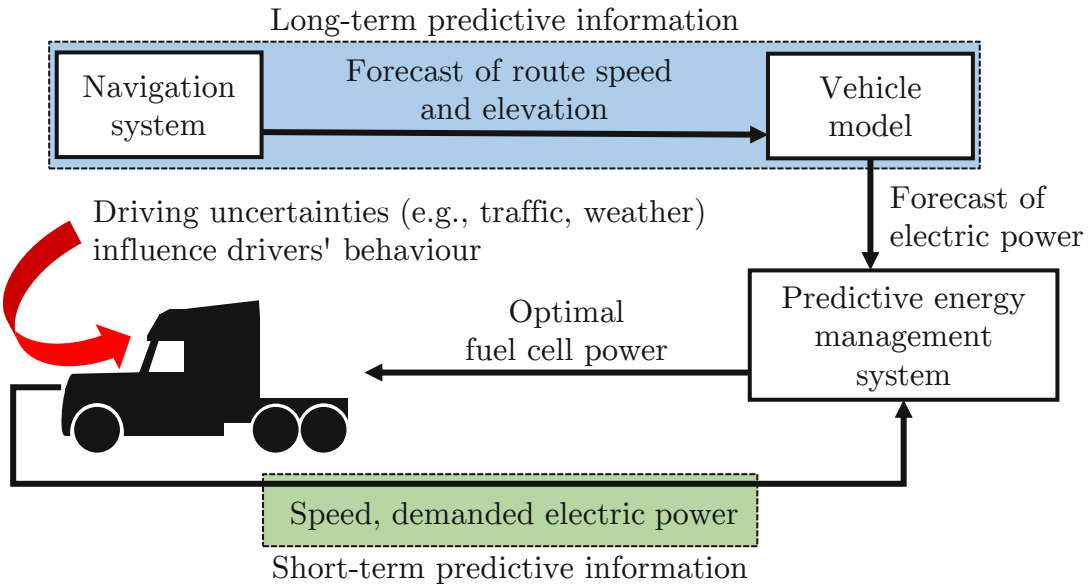


Figure 1.1: Scheme of the short-term and long-term information processing.

## 1.2 Literature survey

An energy management system of an FCEV determines the optimal power-split between multiple energy sources depending on control objectives. This represents a challenging task due to various requirements (e.g., availability of high-performance real-time hardware, real-time controllability etc.) and efficiency criteria (e.g., state of charge control, fuel consumption, battery degradation etc.).
In general, EMS can be classified in rule-based (also referred as *heuristic*) and model-based optimisation methods (also referred as *optimal*) [4] [5]. Heuristic strategies are based on engineering intuition, and correlations involving various vehicular variables [5]. Model-based strategies, on the other hand, rely on mathematical models and systematic optimisation procedures to find (local) minima [5]. Rule-based strategies (RBS) are easy to implement and widely used but often result in suboptimal solutions. On the contrary, model-based strategies are hard to be implemented in real-time control systems, although they overcome the inherent drawback of RBS [6]. For this reason, research focuses on improving the optimality of rule-based energy management strategy and reducing the computation load of model-based energy management strategy [6].
One approach for designing a predictive energy management system, widely used in the literature, is to calculate a reference trajectory based on long-term information, constraints and prediction objectives. Furthermore, the reference is used as a final-state constraint, either by a rule-based or a model-based optimisation.
Sun et al. [7] proposes a predictive energy management strategy that integrates real-time traffic data. With this data, the traffic flow velocity can be obtained, followed by the calculation of the optimal SoC trajectory. The MPC uses the horizon velocity predictor and the SoC reference to forecast the future driving velocities in each receding horizon. These two aspects correspond to long-term and short-term disturbances, respectively. The simulation results show that fuel optimality can be achieved.
Lim et al. [8] proposes a distance-based eco-driving scheme using a two-stage hierarchy for long-term optimisation and local adaptation. Before departure, a speed profile is calculated in a distance domain for the entire driving route. While driving, the previous and current speed of the vehicle ahead and the current distance to the preceding vehicle is used to estimate the future distance to the car. The speed is adjusted if the distance is below a certain safety threshold. This approach minimises the computing time for real-time applications while ensuring a long-term balance between fuel consumption and driving time.
Zendegan et al. [9] proposes a method to use basic route information like speed limits and route topography to estimate the electrical power demand. A location-based SoC reference signal is obtained using the prediction with quadratic programming. A rule-based approach is used to track the reference trajectory during online energy man-

agement implementation. This predictive strategy improves the fuel economy, SoC control, and the system lifetime.
Xie et al. [10] combines short-term and long-term information by proposing an integrated vehicle trajectory prediction method using multiple models. A physics-based model and manoeuvre-based model are used to predict vehicle trajectories. While the first model is based on a kinematic motion model, the latter is based on the dynamic Bayesian network to infer the driving manoeuvres. Combining the two models achieves short-term accuracy by considering the vehicle running dynamic parameters and provides long-term insight into future trajectories by estimating manoeuvres.
One possible approach for combining short-term and long-term information is to use model predictive control to consider the near and far future. It can be used to calculate an optimal control sequence that minimises the cost function while considering constraints. A high prediction horizon increases computational complexity, and it cannot be used for real-time operation. Consequently, a solution needs to be found on how to modify and adapt a model predictive control.
A real-time management strategy for an electric vehicle is developed by Gomozov et al. [11]. An MPC-based energy management strategy is introduced that benefits from both short-term and long-term prediction using non-uniformly distributed sampling times. As the discrete state-space model is formulated beforehand, the distribution of the sampling time is not changed during the simulation. This approach allows for a fast dynamics control of the supercapacitor and the long-term prediction of power demand while minimising the computational load and enabling the online implementation of the MPC.

## 1.3 Contribution and outline

This thesis proposes a novel MPC formulation as a PEMS with long prediction horizons but few decision variables. In particular, the classical MPC formulation is modified to have non-uniformly distributed control variables. While the length of the prediction horizon significantly impacts the simulation time, it also reduces the hydrogen consumption for the heavy-duty vehicle. However, increasing the number of control variables does not necessarily result in better fuel economy. Since the weight matrices of the cost function are chosen to achieve comparability between various prediction horizons, the results' robustness depends on the used driving cycle.
This thesis is organised as follows: In Section 2, the heavy-duty fuel cell vehicle is described. In Section 3, the predictive energy management system is presented. in Section 4, the simulation results are provided, analysed and validated. The conclusions are given in Section 5

# Chapter 2

# Heavy-duty fuel cell vehicle

A basic framework must first be defined to formulate energy and power management. This chapter presents the basic configuration of the heavy-duty fuel cell vehicle used in this thesis. After an overview of the powertrain configuration, the component model approaches from the literature are reviewed, and the chosen models are presented.

## 2.1 Powertrain architecture

Figure 2.1 depicts the simplified architecture of the powertrain of the fuel cell electric vehicle. The electric motor and the fuel cell system, including the fuel cell stack and auxiliary functions such as air compressor and humidifiers, are connected to a DC bus through power converters. The battery system is directly linked to the powertrain. The battery can be recharged by the fuel cell or regenerative braking energy. However, the necessary heating and cooling system (e.g., cooling trucks, air conditioning) is not depicted, but it is considered in the auxiliary loads $P_{aux}$.

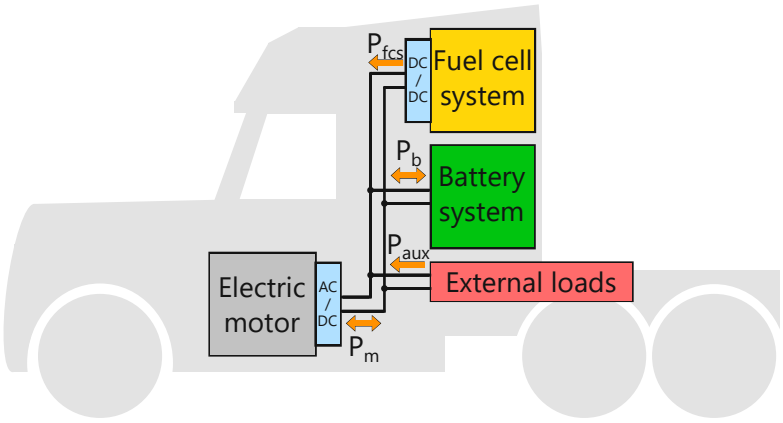


Figure 2.1: Architecture of the electric powertrain of the vehicle.

All parameters and constraints of the vehicle model are listed in Table 2.1.

Table 2.1: Parameters and constraints

| Parameter | Symbol | Value |
|---|---|---|
| Vehicle mass | $m_v$ | 35 000 kg |
| Gravitational acceleration | g | 9.81 m/s$^2$ |
| Rolling friction coefficient at 0 km/h | $c_r$ | 0.005522 kg |
| Rolling friction coefficient at 100 km/h | $c_r$ | 0.008144 kg |
| Vehicle frontal area | $A_v$ | 9.57 m$^2$ |
| Drag coefficient | $c_x$ | 0.58 |
| Air density | $\rho_{air}$ | 1.2 kg/m$^3$ |
| Total efficiency | $\eta_T$ | 0.87 |
| Auxiliary loads | $P_{aux}$ | 11500 W |
| Optimal fuel cell power | $P_{fcs,ref}$ | 57811 W |
| Minimum fuel cell power | $P_{fcs,min}$ | 1 W |
| Maximum fuel cell power | $P_{fcs,max}$ | 320000 W |
| Hydrogen lower heating value | LHV | 120 MJ/kg |
| Minimum charging power battery | $P_{b,min}$ | -106920 W |
| Maximum charging power battery | $P_{b,max}$ | 427680 W |
| Battery nominal energy | $E_{b,nom}$ | 53.46 kWh |
| State of energy reference | $SoE_{ref}$ | 0.65 |
| State of energy maximum | $SoE_{max}$ | 0.9 |
| State of energy minimum | $SoE_{min}$ | 0.4 |

## 2.2 Modelling

Models of physical components are required to adequately represent a target system for analysis and simulation. Since the model approaches available in the literature vary in complexity and dimension, a brief overview and comparison will be given.

### 2.2.1 Longitudinal model

To describe the behaviour of vehicle dynamics, a simple longitudinal model is used (see Figure 2.2).

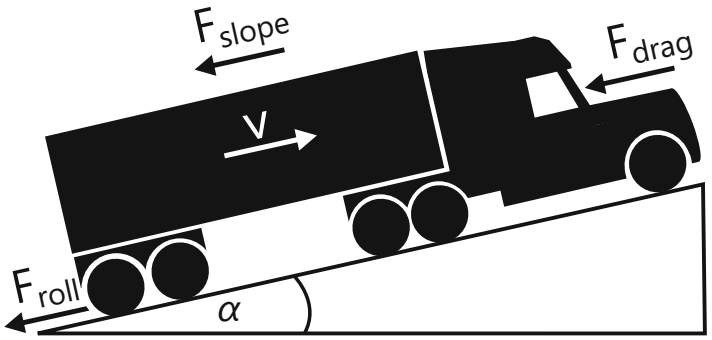


Figure 2.2: Scheme of vehicle longitudinal dynamics.

Basically, the resultant force $F_{res}$ acting on the vehicle is calculated by the resistance force $F_{roll}$, the force due the slope of the driving cycle $F_{slope}$ and the drag force $F_{drag}$. These forces are given in (2.2), (2.3) and (2.4).

$$F_{res} = F_{roll} + F_{slope} + F_{drag} \tag{2.1}$$

$$F_{roll} = m_v \cdot g \cdot c_r \cdot \cos\alpha \tag{2.2}$$

$$F_{slope} = m_v \cdot g \cdot \sin\alpha \tag{2.3}$$

$$F_{drag} = \frac{1}{2} \cdot A_v \cdot c_x \cdot \rho_{air} \cdot v^2 \tag{2.4}$$

The power at wheels $P_w$ is calculated as follows:

$$P_w = (m_v \cdot \dot{v} + F_{res}) \cdot v \tag{2.5}$$

The electric load $P_{el}$ is calculated in (2.6). For simplicity, the auxiliary loads $P_{aux}$ are assumed constant. Also, the average total efficiency $\eta_T$ is a constant value because power losses due to the electric motor or drivetrain components are not relevant for this thesis.

$$P_{el} = P_{aux} + P_w \cdot \eta_T^{-sign(P_w)} \tag{2.6}$$

The longitudinal model is embedded in a forward-facing simulation approach. A driver model sends an acceleration or brake signal to the powertrain to follow the desired speed profile from the drive cycle. The driver model modifies its commands to minimise the

error between the actual vehicle speed and the desired speed. Still, inevitably a tiny margin of error between these two velocity profiles will always occur [12]. This approach is used in this thesis.
A different approach is a backwards-facing simulation. The required power is calculated directly in the vehicle model based on the speed profile. The needed power is then used to calculate the necessary torque and imposed onto the powertrain components. In such an approach, the power flow is calculated backwards through the power train, without a driver model [12].
In conclusion, the forward simulation uses the available system resources. It represents the behaviour of an actual vehicle and driver, while a backward simulation approach can help find the system's optimum design specifications.

### 2.2.2 Fuel cell system

Various factors affect the overall performance of a proton-exchange membrane fuel cell (PEMFC). The energetic performance of a PEMFC depends on its operating conditions (e.g. temperature, pressure, ageing and degradation phenomena).
Many fuel cell models have developed over the past years. The existing PEMFC models can be categorised into black box, grey box and white box models. Black-box models are based only on experimental data, and white-box models are based solely on algebraic and differential equations. Grey box models combine the previously stated models, and they are based on empirical equations backed up by experimental data [13].
For this thesis, the required model should be usable for a predictive energy management system while authentically representing an entire fuel cell system. A simplified static model is considered, where the fuel cell system power is the difference between stack power and auxiliaries losses, like a compressor or cooling fan (see Ferrara et al. [14]).

The chosen static model neglects the system response time. Therefore, the system efficiency only depends on the fuel cell power. In Figure 2.3 the efficiency and hydrogen consumption depending on the power are shown. Since the model provides adequate results for investigations of a predictive energy management system of FCEVs (see [14], [15], [9]), it is sufficient for this thesis.

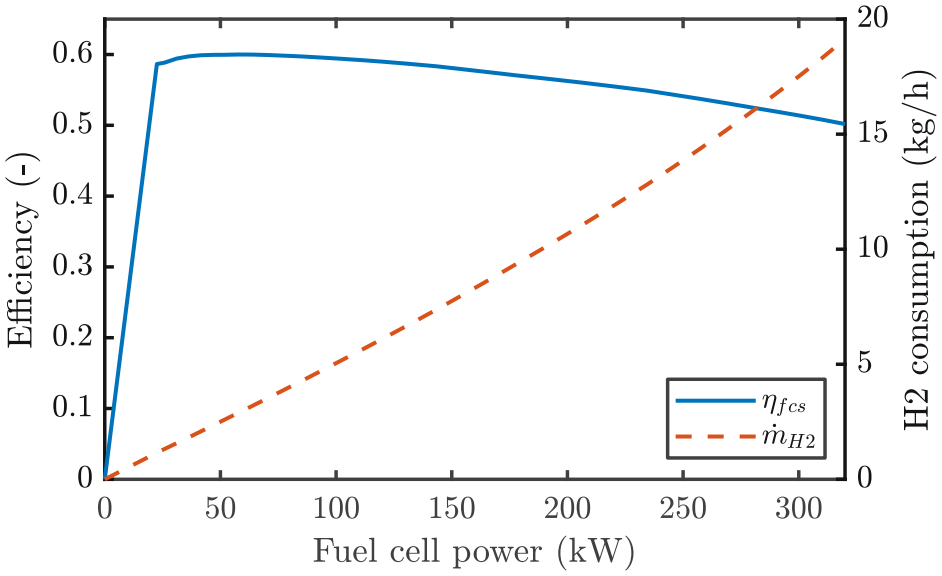


Figure 2.3: Fuel cell efficiency and hydrogen consumption.

### 2.2.3 Battery model

Various approaches to battery models can be found in the literature as different application areas determine the model's objectives (e.g., battery design, state of charge estimation, thermal analysis). One major group of battery models consist of electrochemical models. They are based on chemical reactions occurring inside the battery cells. This model is the most accurate one, but due to the complexity of the nonlinear differential equations, it is not useful in terms of vehicular applications [16]. It is possible to use a mathematical model to describe the battery properties, and such models can be classified into stochastic or analytical models. Stochastic models are based on discrete-time Markov chain. A Markov process predicts possible events of the process depending on its present state. Such a solution is still accurate compared to electrochemical models, but their computation is faster.

For an analytical approach, heuristic knowledge or empirical formulas are used to model specific characteristics of batteries [17]. However, these models are not useful for SoC estimation, or real-time control [18]. Equivalent electrical circuit models use electrical components to model the behaviour of a battery. Due to its simplicity, it's used for dynamic simulations of hybrid, and electric vehicles [18]. Therefore, an equivalent electrical circuit model is used for an SoE estimation in this thesis (see [14]).
The ideal voltage source $V_{oc}$ is connected in series with a resistor, representing the battery internal resistance $R_{int}$, as shown in Figure 2.4. Due to simplicity, both are assumed as constant.

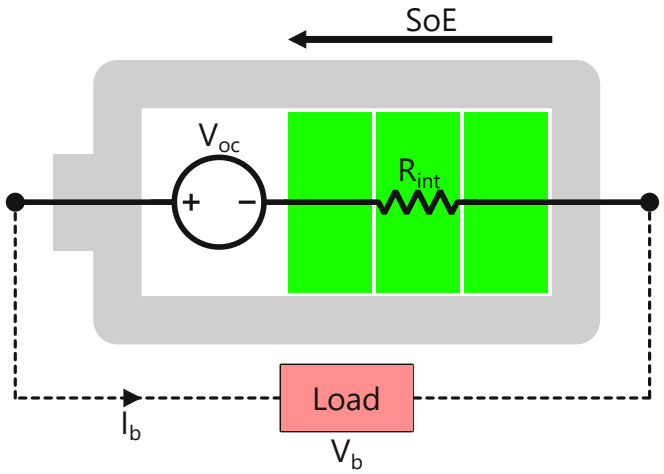


Figure 2.4: Equivalent circuit of the battery system.

The battery terminal voltage $V_b$ is calculated by (2.7). The battery current $I_b$ is positive in discharging operation.

$$V_b = V_{oc} - R_{int} \cdot I_b \tag{2.7}$$

Therefore, the battery power is computed in the following way:

$$P_b = (V_{oc} - R_{int} \cdot I_b) \cdot I_b \tag{2.8}$$

The state of energy of the battery is used to indicate the current state of the battery. It is defined as:

$$\frac{\mathrm{d}SoE(t)}{\mathrm{d}t} = -P_b \cdot \frac{\Delta t}{E_{b,nom}} \tag{2.9}$$

where $\Delta t$ denotes the sampling time and $E_{b,nom}$ denotes the battery nominal energy.

## 2.3 Realistic driving cycles

In Figure 2.5, speed, elevation and the electrical power demand of a real-world driving cycle are depicted. The dotted horizontal lines show the maximum and minimum fuel cell power in the bottom figure. At certain times the electrical power demand is higher than the maximum fuel cell power (e.g. t=110s). If only fuel cell utilisation is available, the demand for electrical power cannot be met, and the vehicle needs to decelerate or stop. In addition, a battery can be recharged by absorbing the kinetic energy from the mechanical braking process. An energy management system for a fuel cell electric vehicle must distribute the demanded load between the fuel cell and battery while maintaining a state of energy control to charge and discharge the battery at the correct times.

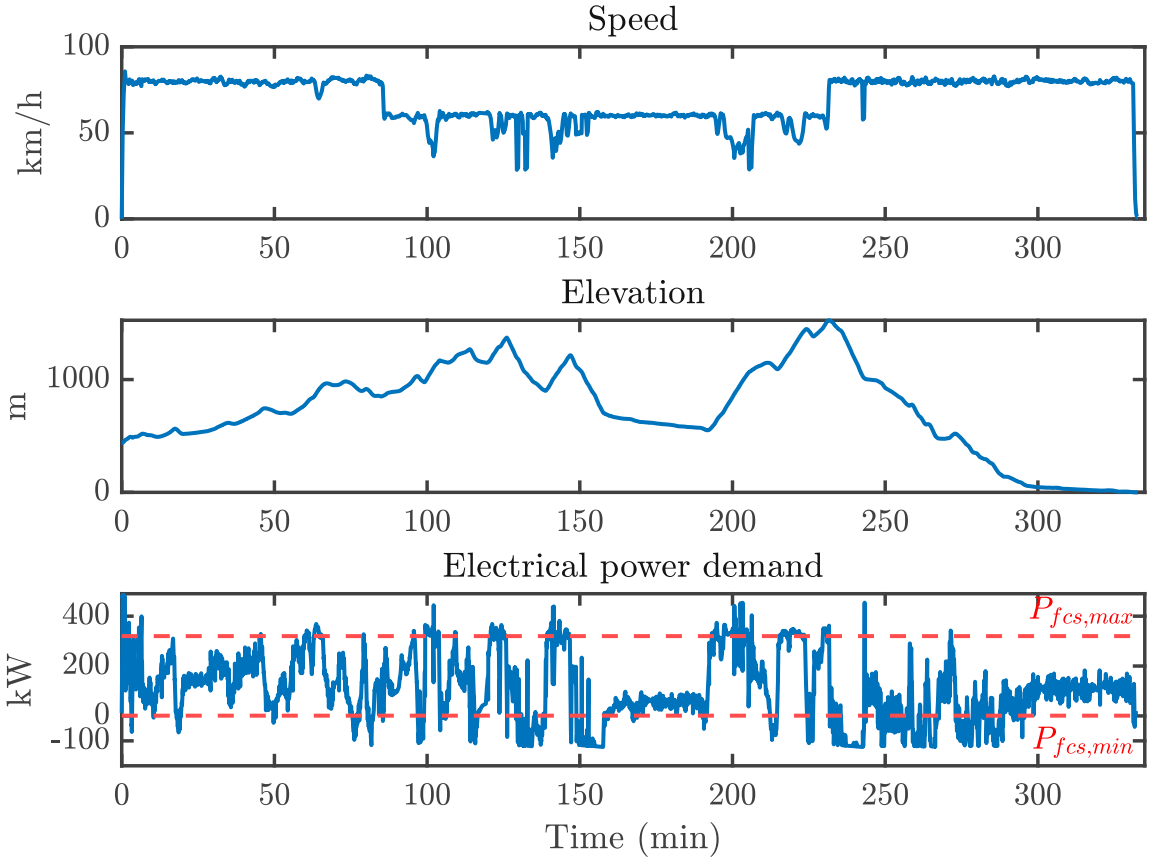


Figure 2.5: Driving cycle B: speed (top), elevation (middle), electrical power demand (bottom).

# Chapter 3

# Predictive energy management system

This chapter is about formulating the new concept of the model predictive controller, describing the state-space model, defining how predictive information is processed and modified, and how energy management strategy is implemented.

## 3.1 Model predictive control

### Combining short-term and long-term information

There is a trade-off between the proper prediction horizon length for an MPC. Compared to a short prediction horizon, a high prediction horizon allows for a longer foresight of the future states, but the computational complexity increases. Long-term predictive information of the future road conditions is necessary for optimal SoC control. However, short-term predictive information compensates for driving uncertainties (e.g., traffic flow speed).
The purpose of the new concept for MPC is to use a long-term power demand forecast based on a driving cycle's velocity and elevation profile while incorporating short-term information like driver's behaviour into calculating optimal fuel cell power.
However, combining short-term and long-term information while minimising computational complexity requires modifying the basic formulation of an MPC.

The principle of model predictive control is the prediction of future outputs at each instant k for the prediction horizon $N_p$, using the process model (see Figure 3.1). The predicted outputs $\boldsymbol{y}(k+i|k)$ depend on the past inputs and outputs up to instant k and on the future control signal $\boldsymbol{u}(k+j|k)$, where i = 1,2...Np and j = 0,1...Nc-1.
The goal of an MPC is to minimise the error between the reference trajectory and the output.

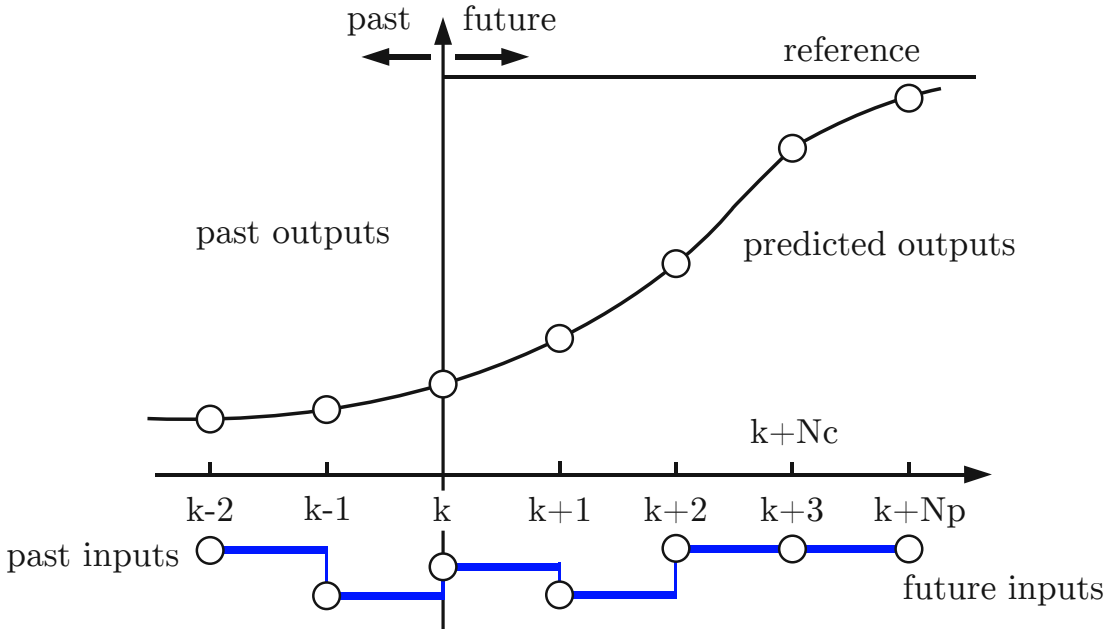


Figure 3.1: Basic principle of model based predictive control.

With the standard formulation, the control variables are equidistant and act at every time step till t=k+Nc (see Figure 3.1). If one wants to use a model predictive control for short-term and long-term prediction, the control horizon must be either high or equal to the prediction horizon. This is possible, but the matrices' size increase and the calculation's complexity make a classical MPC unusable for online implementation.

The basic idea of the new concept for MPC is depicted in Figure 3.2. If one compares Figure 3.1 with Figure 3.2, it can be easily seen that the future inputs are not equally distributed over the horizon. At the same time, the outputs are still predicted for every time step. It is possible to have a high $N_p$ while using a small number of control variables that are distributed over the entire horizon. With a high density of control variables in the near future and only a few in the far future, the initial goal to combine short-term and long-term information is achieved.

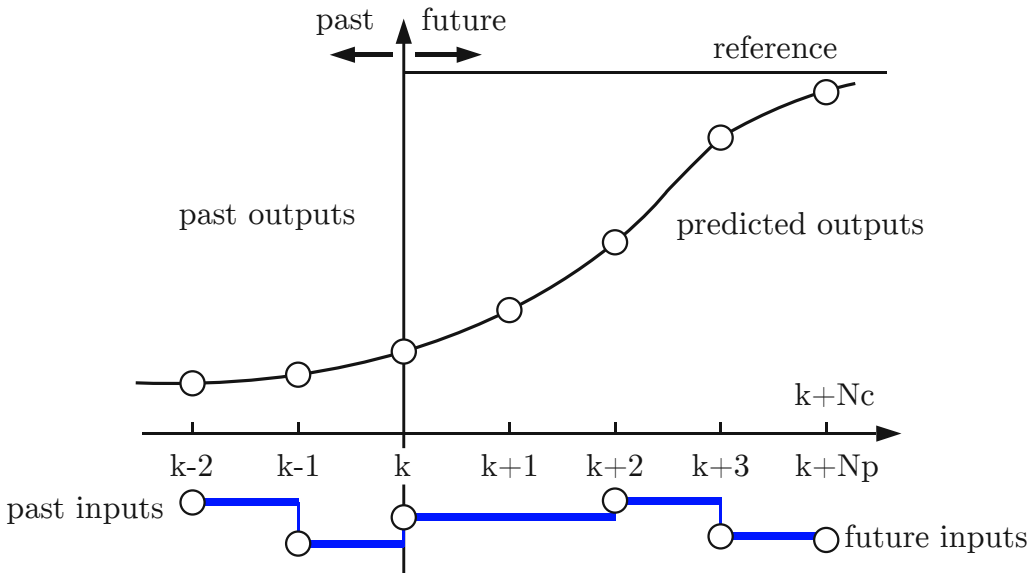


Figure 3.2: New concept for model based predictive control.

While the predicted outputs $\boldsymbol{y}(k+i|k)$ still depend on the past inputs and outputs up to instant k, the dependency on the future control signal $\boldsymbol{u}(k+j|k)$ is reduced as the control variables are neglected for specific time steps. This presents a challenge for the processing of predictive information. Therefore the MPC needs adapted prediction information (see section 3.3).

## Basic concept of model predictive control

The formulation for the predicted variables in terms of current state variable information and the future control increments is used to derive the new approach.
First, based on a state-space model, the future state variables are calculated sequentially using the set of future control parameters:

$$\begin{aligned}
\boldsymbol{x}(k+1|k) &= \boldsymbol{A}\cdot\boldsymbol{x}(k)+\boldsymbol{B}\cdot\Delta u(k)+\boldsymbol{E}\cdot\Delta z(k)\\
\boldsymbol{x}(k+2|k) &= \boldsymbol{A}\cdot\boldsymbol{x}(k+1|k)+\boldsymbol{B}\cdot\Delta u(k+1)+\boldsymbol{E}\cdot\Delta z(k+1)\\
&= \boldsymbol{A}^2\cdot\boldsymbol{x}(k)+\boldsymbol{A}\cdot\boldsymbol{B}\cdot\Delta u(k)+\boldsymbol{B}\cdot\Delta u(k+1)\\
&\quad +\boldsymbol{A}\cdot\boldsymbol{E}\cdot\Delta z(k)+\boldsymbol{E}\cdot\Delta z(k+1)\\
&\quad .\\
&\quad .\\
&\quad .\\
\boldsymbol{x}(k+Np|k) &= \boldsymbol{A}^{Np}\cdot\boldsymbol{x}(k)\\
&\quad +\boldsymbol{A}^{Np-1}\cdot\boldsymbol{B}\cdot\Delta u(k)+\boldsymbol{A}^{Np-2}\cdot\boldsymbol{B}\cdot\Delta u(k+1)\cdots\\
&\quad +\boldsymbol{A}^{Np-Nc}\cdot\boldsymbol{B}\cdot\Delta u(k+Nc-1)\\
&\quad +\boldsymbol{A}^{Np-1}\cdot\boldsymbol{E}\cdot\Delta z(k)+\boldsymbol{A}^{Np-2}\cdot\boldsymbol{E}\cdot\Delta z(k+1)\cdots\\
&\quad +\boldsymbol{E}\cdot\Delta z(k+Np-1)
\end{aligned}$$

The prediction is given by:

$$\begin{aligned}
\boldsymbol{y}(k+1|k) &= \boldsymbol{C}\cdot\boldsymbol{A}\cdot\boldsymbol{x}(k)+\boldsymbol{C}\cdot\boldsymbol{B}\cdot\Delta u(k)+\boldsymbol{C}\cdot\boldsymbol{E}\cdot\Delta z(k)\\
\boldsymbol{y}(k+2|k) &= \boldsymbol{C}\cdot\boldsymbol{A}\cdot\boldsymbol{x}(k+1|k)+\boldsymbol{C}\cdot\boldsymbol{B}\cdot\Delta u(k+1)+\boldsymbol{C}\cdot\boldsymbol{E}\cdot\Delta z(k+1)\\
&= \boldsymbol{C}\cdot\boldsymbol{A}^2\cdot\boldsymbol{x}(k)+\boldsymbol{C}\cdot\boldsymbol{A}\cdot\boldsymbol{B}\cdot\Delta u(k)+\boldsymbol{C}\cdot\boldsymbol{B}\cdot\Delta u(k+1)\\
&\quad +\boldsymbol{C}\cdot\boldsymbol{A}\cdot\boldsymbol{E}\cdot\Delta z(k)+\boldsymbol{C}\cdot\boldsymbol{E}\cdot\Delta z(k+1)\\
&\quad .\\
&\quad .\\
&\quad .\\
\boldsymbol{y}(k+Np|k) &= \boldsymbol{C}\cdot\boldsymbol{A}^{Np}\cdot\boldsymbol{x}(k)\\
&\quad +\boldsymbol{C}\cdot\boldsymbol{A}^{Np-1}\cdot\boldsymbol{B}\cdot\Delta u(k)+\boldsymbol{C}\cdot\boldsymbol{A}^{Np-2}\cdot\boldsymbol{B}\cdot\Delta u(k+1)\cdots\\
&\quad +\boldsymbol{C}\cdot\boldsymbol{A}^{Np-Nc}\cdot\boldsymbol{B}\cdot\Delta u(k+Nc-1)\\
&\quad +\boldsymbol{C}\cdot\boldsymbol{A}^{Np-1}\cdot\boldsymbol{E}\cdot\Delta z(k)+\boldsymbol{C}\cdot\boldsymbol{A}^{Np-2}\cdot\boldsymbol{E}\cdot\Delta z(k+1)\cdots\\
&\quad +\boldsymbol{C}\cdot\boldsymbol{E}\cdot\Delta z(k+Np-1)
\end{aligned}$$

Defining the vectors:

$$\boldsymbol{Y}=\begin{bmatrix} y(k+1|k)\\ y(k+2|k)\\ y(k+3|k)\\ \vdots\\ y(k+Np|k)\end{bmatrix},\boldsymbol{\Delta U}=\begin{bmatrix}\Delta u(k)\\ \Delta u(k+1)\\ \Delta u(k+2)\\ \vdots\\ \Delta u(k+Nc-1)\end{bmatrix},\boldsymbol{\Delta Z}=\begin{bmatrix}\Delta z(k)\\ \Delta z(k+1)\\ \Delta z(k+2)\\ \vdots\\ \Delta z(k+Np-1)\end{bmatrix} \tag{3.1}$$

One can formulate the expressions in a compact matrix form as:

$$\boldsymbol{Y} = \boldsymbol{F} \cdot \boldsymbol{x}(k) + \boldsymbol{\Phi_u} \cdot \boldsymbol{\Delta U} + \boldsymbol{\Phi_z} \cdot \boldsymbol{\Delta Z} \tag{3.2}$$

where

$$\boldsymbol{F} = \begin{bmatrix} \boldsymbol{C} \cdot \boldsymbol{A} \\ \boldsymbol{C} \cdot \boldsymbol{A}^2 \\ \boldsymbol{C} \cdot \boldsymbol{A}^3 \\ \vdots \\ \boldsymbol{C} \cdot \boldsymbol{A}^{Np} \end{bmatrix}, \tag{3.3}$$

$$\boldsymbol{\Phi_u} = \begin{bmatrix} \boldsymbol{C} \cdot \boldsymbol{B} & \boldsymbol{0} & \boldsymbol{0} & \cdots & \boldsymbol{0} \\ \boldsymbol{C} \cdot \boldsymbol{A} \cdot \boldsymbol{B} & \boldsymbol{C} \cdot \boldsymbol{B} & \boldsymbol{0} & \cdots & \boldsymbol{0} \\ \boldsymbol{C} \cdot \boldsymbol{A}^2 \cdot \boldsymbol{B} & \boldsymbol{C} \cdot \boldsymbol{A} \cdot \boldsymbol{B} & \boldsymbol{C} \cdot \boldsymbol{B} & \cdots & \boldsymbol{0} \\ \vdots & \vdots & \vdots & \ddots & \vdots \\ \boldsymbol{C} \cdot \boldsymbol{A}^{Np-1} \cdot \boldsymbol{B} & \boldsymbol{C} \cdot \boldsymbol{A}^{Np-2} \cdot \boldsymbol{B} & \boldsymbol{C} \cdot \boldsymbol{A}^{Np-3} \cdot \boldsymbol{B} & \cdots & \boldsymbol{C} \cdot \boldsymbol{A}^{Np-Nc} \cdot \boldsymbol{B} \end{bmatrix} \tag{3.4}$$

$$\boldsymbol{\Phi_z} = \begin{bmatrix} \boldsymbol{C} \cdot \boldsymbol{E} & \boldsymbol{0} & \boldsymbol{0} & \cdots & \boldsymbol{0} \\ \boldsymbol{C} \cdot \boldsymbol{A} \cdot \boldsymbol{E} & \boldsymbol{C} \cdot \boldsymbol{E} & \boldsymbol{0} & \cdots & \boldsymbol{0} \\ \boldsymbol{C} \cdot \boldsymbol{A}^2 \cdot \boldsymbol{E} & \boldsymbol{C} \cdot \boldsymbol{A} \cdot \boldsymbol{E} & \boldsymbol{C} \cdot \boldsymbol{E} & \cdots & \boldsymbol{0} \\ \vdots & \vdots & \vdots & \ddots & \vdots \\ \boldsymbol{C} \cdot \boldsymbol{A}^{Np-1} \cdot \boldsymbol{E} & \boldsymbol{C} \cdot \boldsymbol{A}^{Np-2} \cdot \boldsymbol{E} & \boldsymbol{C} \cdot \boldsymbol{A}^{Np-3} \cdot \boldsymbol{E} & \cdots & \boldsymbol{C} \cdot \boldsymbol{E} \end{bmatrix} \tag{3.5}$$

The matrices $\boldsymbol{\Phi_z}$ and $\boldsymbol{\Phi_u}$ have a block Toeplitz structure. In Table 3.1 the dimension of the matrices is shown, where Np is the prediction horizon, Nc is the control horizon, nz is the number of disturbances, nu is the number of inputs and ny is the number of outputs.

Table 3.1: Size of matrices

| Variable | Size |
|---|---|
| $\boldsymbol{\Phi_z}$ | $(Np \cdot ny) \times (Np \cdot nz)$ |
| $\boldsymbol{\Phi_u}$ | $(Np \cdot ny) \times (Nc \cdot nu)$ |
| $\boldsymbol{\Delta Z}$ | $Np \times nz$ |
| $\boldsymbol{\Delta U}$ | $Nc \times ny$ |
| $\boldsymbol{Y}$ | $Np \times ny$ |

## New concept for model predictive control

Table 3.1 shows that a high prediction horizon has a huge impact on the size of the matrices. If the whole prediction horizon should be controllable, both horizons have the same length (Np = Nc). Thus, all matrices become large, and the computational complexity rises. Hence, an useful online implementation is not possible anymore. This thesis proposes a model predictive control with not-equidistant distributed control variables over the entire prediction horizon to solve this problem.
Before providing the general form of the new matrices, the approach is demonstrated by the following example: assuming a SISO System with a prediction horizon of 5 seconds and two control variables, which act at t=1s and t=4s. A new variable is introduced that specifies in which time steps the control and disturbance variables act:

$$\boldsymbol{Ncs} = \begin{bmatrix} k \\ k+3 \end{bmatrix} \tag{3.6}$$

First, the disturbance increments are assumed to affect the future variables at the same time steps as the control increments. Therefore, both vectors have the same size. With this information $\boldsymbol{\Delta U}$ and $\boldsymbol{\Delta Z}$ can be assembled:

$$\boldsymbol{\Delta U} = \begin{bmatrix} \Delta u(k) \\ 0 \\ 0 \\ \Delta u(k+3) \\ 0 \end{bmatrix}, \boldsymbol{\Delta Z} = \begin{bmatrix} \Delta z(k) \\ 0 \\ 0 \\ \Delta z(k+3) \\ 0 \end{bmatrix} \tag{3.7}$$

Now the steps to calculate sequentially the future state space vectors can be repeated. This leads to:

$$\boldsymbol{\Phi_u} = \begin{bmatrix} \boldsymbol{C \cdot B} & 0 & 0 & 0 & 0 \\ \boldsymbol{C \cdot A \cdot B} & 0 & 0 & 0 & 0 \\ \boldsymbol{C \cdot A^2 \cdot B} & 0 & 0 & 0 & 0 \\ \boldsymbol{C \cdot A^3 \cdot B} & 0 & 0 & \boldsymbol{C \cdot B} & 0 \\ \boldsymbol{C \cdot A^4 \cdot B} & 0 & 0 & \boldsymbol{C \cdot A \cdot B} & 0 \end{bmatrix}$$

$$\boldsymbol{\Phi_z} = \begin{bmatrix} \boldsymbol{C \cdot E} & 0 & 0 & 0 & 0 \\ \boldsymbol{C \cdot A \cdot E} & 0 & 0 & 0 & 0 \\ \boldsymbol{C \cdot A^2 \cdot E} & 0 & 0 & 0 & 0 \\ \boldsymbol{C \cdot A^3 \cdot E} & 0 & 0 & \boldsymbol{C \cdot E} & 0 \\ \boldsymbol{C \cdot A^4 \cdot E} & 0 & 0 & \boldsymbol{C \cdot A \cdot E} & 0 \end{bmatrix} \tag{3.8}$$

All zero-columns of $\boldsymbol{\Phi_u}$ and $\boldsymbol{\Phi_z}$ and the corresponding zero-rows of $\boldsymbol{\Delta U}$ and $\boldsymbol{\Delta Z}$, respectively, can be removed. This results to:

$$\boldsymbol{\Delta U} = \begin{bmatrix} \Delta u(k) \\ \Delta u(k+3) \end{bmatrix}, \boldsymbol{\Delta Z} = \begin{bmatrix} \Delta z(k) \\ \Delta z(k+3) \end{bmatrix} \tag{3.9}$$

$$\boldsymbol{\Phi_u} = \begin{bmatrix} \boldsymbol{C \cdot B} & 0 \\ \boldsymbol{C \cdot A \cdot B} & 0 \\ \boldsymbol{C \cdot A^2 \cdot B} & 0 \\ \boldsymbol{C \cdot A^3 \cdot B} & \boldsymbol{C \cdot B} \\ \boldsymbol{C \cdot A^4 \cdot B} & \boldsymbol{C \cdot A \cdot B} \end{bmatrix}, \boldsymbol{\Phi_z} = \begin{bmatrix} \boldsymbol{C \cdot E} & 0 \\ \boldsymbol{C \cdot A \cdot E} & 0 \\ \boldsymbol{C \cdot A^2 \cdot E} & 0 \\ \boldsymbol{C \cdot A^3 \cdot E} & \boldsymbol{C \cdot E} \\ \boldsymbol{C \cdot A^4 \cdot E} & \boldsymbol{C \cdot A \cdot E} \end{bmatrix} \tag{3.10}$$

This example shows that it is not necessary to calculate sequentially the future state space, but rather a compact matrix formulation can be provided: $\boldsymbol{Ncs}$ specifies in which time steps the control and disturbance variables act:

$$\boldsymbol{Ncs} = \begin{bmatrix} k \\ k+j \\ k+j \\ \vdots \\ k+j \end{bmatrix}, \text{where j = 1,2...Np-1} \tag{3.11}$$

$\mathbf{Ncs}(n)$ specifies for the $n^{th}$ column of $\boldsymbol{\Phi_u}$ or $\boldsymbol{\Phi_z}$ and the $n^{th}$ row of $\boldsymbol{\Delta U}$ and $\boldsymbol{\Delta Z}$, where n = 1,2...Nc.
$\mathbf{0}_u$ and $\mathbf{0}_z$, respectively, represent a zero matrix with dimension $(ny \cdot Ncs(n)) \times nu)$ and $((ny \cdot Ncs(n)) \times nz)$. It is assumed that the first variable of the predicted output is not neglected and therefore the first column has no zero values. This means that $\mathbf{Ncs}(1)$ always has the value 1. The matrices $\boldsymbol{\Phi_u}$ and $\boldsymbol{\Phi_z}$ be assembled in the following way:

$$\boldsymbol{\Phi_u} = \begin{bmatrix} \boldsymbol{C \cdot B} & \mathbf{0}_u & \cdots & \mathbf{0}_u \\ \boldsymbol{C \cdot A \cdot B} & \boldsymbol{C \cdot B} & \cdots & \boldsymbol{C \cdot B} \\ \boldsymbol{C \cdot A^2 \cdot B} & \boldsymbol{C \cdot A \cdot B} & \cdots & \boldsymbol{C \cdot A \cdot B} \\ \vdots & \vdots & \vdots & \vdots \\ \boldsymbol{C \cdot A^{Np-Ncs(1)} \cdot B} & \boldsymbol{C \cdot A^{Np-Ncs(2)} \cdot B} & \cdots & \boldsymbol{C \cdot A^{Np-Ncs(Nc)} \cdot B} \end{bmatrix} \tag{3.12}$$

$$\boldsymbol{\Phi_z} = \begin{bmatrix} \boldsymbol{C \cdot E} & \mathbf{0}_z & \cdots & \mathbf{0}_z \\ \boldsymbol{C \cdot A \cdot E} & \boldsymbol{C \cdot E} & \cdots & \boldsymbol{C \cdot E} \\ \boldsymbol{C \cdot A^2 \cdot E} & \boldsymbol{C \cdot A \cdot E} & \cdots & \boldsymbol{C \cdot A \cdot E} \\ \vdots & \vdots & \vdots & \vdots \\ \boldsymbol{C \cdot A^{Np-Ncs(1)} \cdot E} & \boldsymbol{C \cdot A^{Np-Ncs(2)} \cdot E} & \cdots & \boldsymbol{C \cdot A^{Np-Ncs(Nc)} \cdot E} \end{bmatrix} \tag{3.13}$$

In Table 3.2 a comparison of the dimension size of the matrices between the basic definition and the new concept is documented.

Table 3.2: Comparison: size of matrices

| Variable | Size (basic definition) | Size (new approach) |
|---|---|---|
| $\boldsymbol{\Phi_z}$ | $(Np \cdot ny) \times (Np \cdot nz)$ | $(Np \cdot ny) \times (Nc \cdot nz)$ |
| $\boldsymbol{\Phi_u}$ | $(Np \cdot ny) \times (Nc \cdot nu)$ | $(Np \cdot ny) \times (Nc \cdot nu)$ |
| $\boldsymbol{\Delta Z}$ | $Np \times nz$ | $Nc \times nz$ |
| $\boldsymbol{\Delta U}$ | $Nc \times ny$ | $Nc \times ny$ |
| $\boldsymbol{Y}$ | $Np \times ny$ | $Np \times ny$ |
| $\boldsymbol{Ncs}$ | - | $Nc \times ny$ |

It can be seen that for $\boldsymbol{\Phi_z}$ and $\boldsymbol{\Delta Z}$, the dimension has been reduced. Due to the new approach, Nc no longer specifies the control horizon. The whole prediction horizon can be controlled, so Nc equals the number of control variables for the further thesis.

## 3.2 Predictive energy management strategy

### State space model

First of all, a state-space model is formulated to use the current information about the states of the fuel cell electric vehicle to predict the desired outputs. The electric power is calculated using the power of the battery and the power of the fuel cell:

$$P_{el} = P_b + P_{fcs} \tag{3.14}$$

By inserting (3.14) into (2.9) following formula is obtained:

$$SoE(k+1) = SoE(k) + \frac{\Delta t}{E_{b,nom}} \cdot P_{fcs}(k) - \frac{\Delta t}{E_{b,nom}} \cdot P_{el}(k) \tag{3.15}$$

Taking a difference operation on both sides of (3.15) one gets:

$$\Delta SoE(k+1) = \Delta SoE(k) + b \cdot (\Delta u(k) - \Delta z(k)) \tag{3.16}$$

$$SoE(k+1) = \Delta SoE(k) + SoE(k) + b \cdot (\Delta u(k) - \Delta z(k)) \tag{3.17}$$

$$P_{fcs}(k) = \Delta u(k) + P_{fcs}(k-1) \tag{3.18}$$

$$P_{el}(k) = \Delta z(k) + P_{el}(k-1) \tag{3.19}$$

where $b = \frac{\Delta t}{E_{b,nom}}$, $\Delta u(k) = \Delta P_{fcs}(k)$ and $\Delta z(k) = \Delta P_{el}(k)$.

Now one can formulate the augmented state-space model in compact matrix form:

$$\boldsymbol{x}(k+1) = \boldsymbol{A} \cdot \boldsymbol{x}(k) + \boldsymbol{B} \cdot \Delta u(k) + \boldsymbol{E} \cdot \Delta z(k) \tag{3.20}$$

$$\boldsymbol{y}(k) = \boldsymbol{C} \cdot \boldsymbol{x}(k) \tag{3.21}$$

where

$$\begin{gathered} \boldsymbol{x}(k+1) = \begin{bmatrix} \Delta SoE(k+1) \\ SoE(k+1) \\ P_{fcs}(k) \end{bmatrix}, \boldsymbol{A} = \begin{bmatrix} 1 & 0 & 0 \\ 1 & 1 & 0 \\ 0 & 0 & 1 \end{bmatrix}, \boldsymbol{B} = \begin{bmatrix} b \\ b \\ 1 \end{bmatrix}, \boldsymbol{E} = \begin{bmatrix} -b \\ -b \\ 0 \end{bmatrix}, \\ \boldsymbol{y}(k) = \begin{bmatrix} SoE(k) \\ P_{fcs}(k-1) \end{bmatrix}, \boldsymbol{C} = \begin{bmatrix} 0 & 1 & 0 \\ 0 & 0 & 1 \end{bmatrix} \end{gathered} \tag{3.22}$$

## Cost function

The objective of the predictive control system is to find the best control parameter $\boldsymbol{\Delta U}$ such that an error function between the set-point and the predicted output is minimised [19]. The cost function that achieves the control objective can be found in [19]:

$$J = (\boldsymbol{Y_{ref}} - \boldsymbol{Y})^T \cdot \boldsymbol{Q} \cdot (\boldsymbol{Y_{ref}} - \boldsymbol{Y}) + \boldsymbol{\Delta U}^T \cdot \boldsymbol{R} \cdot \boldsymbol{\Delta U} \tag{3.23}$$

where $\boldsymbol{Q}$ and $\boldsymbol{R}$ are the weight matrices. The optimal $\boldsymbol{\Delta U}$ to minimise J is defined as:

$$\boldsymbol{\Delta U} = (\boldsymbol{\Phi}_u^T \cdot \boldsymbol{\Phi}_u + \boldsymbol{R}^{-1}) \cdot \boldsymbol{\Phi}_u^T \cdot (\boldsymbol{Y_{ref}} - \boldsymbol{F} \cdot \boldsymbol{x}(k) - \boldsymbol{\Phi}_z \cdot \boldsymbol{\Delta Z}) \tag{3.24}$$

There are constraints on the battery and fuel cell system and to guarantee feasible solutions, the definition in [19] is used to implement soft constraints using slack variables:

$$\boldsymbol{M} \cdot \boldsymbol{\Delta U_{slack}} \leq \boldsymbol{\gamma} \tag{3.25}$$

where

$$\boldsymbol{M} = \begin{bmatrix} \boldsymbol{M_1} \\ \boldsymbol{M_2} \end{bmatrix}, \boldsymbol{M_1} = \begin{bmatrix} & -1 & 0 \\ \boldsymbol{\Phi_u} & -1 & 0 \\ & \vdots & \vdots \\ & -1 & 0 \end{bmatrix}, \boldsymbol{M_2} = \begin{bmatrix} & 0 & -1 \\ & 0 & -1 \\ \boldsymbol{\Phi_u} & \vdots & \vdots \\ & 0 & -1 \end{bmatrix} \tag{3.26}$$

$$\boldsymbol{\Delta U_{slack}} = \begin{bmatrix} \boldsymbol{\Delta U} \\ \boldsymbol{s} \end{bmatrix}, \boldsymbol{\gamma} = \begin{bmatrix} \boldsymbol{Y_{min}} + \boldsymbol{F} \cdot \boldsymbol{x}(k) + \boldsymbol{\Phi}_z \cdot \boldsymbol{\Delta Z} \\ \boldsymbol{Y_{max}} - \boldsymbol{F} \cdot \boldsymbol{x}(k) - \boldsymbol{\Phi}_z \cdot \boldsymbol{\Delta Z} \end{bmatrix} \tag{3.27}$$

The reference state of energy value and the highest operational efficiency point of the fuel cell are constant. The vector for set-point information $\boldsymbol{Y_{ref}}$ is defined as follows:

$$\boldsymbol{Y_{ref}} = [SoE_{ref}, P_{fcs,ref}, \ldots, SoE_{ref}, P_{fcs,ref}]^T \tag{3.28}$$

The upper and lower limit for the future outputs are defined as:

$$\boldsymbol{Y_{min}} = [SoE_{min}, P_{fcs,Ymin}(k), \ldots, SoE_{min}, P_{fcs,Ymin}(k+Np-1)]^T \tag{3.29}$$

$$\boldsymbol{Y_{max}} = [SoE_{max}, P_{fcs,Ymax}(k), \ldots, SoE_{max}, P_{fcs,Ymax}(k+Np-1)]^T \tag{3.30}$$

The minimum and maximum value for the fuel cell power are calculated by reformulating (3.14) using the battery constraints:

$$P_{fcs,Ymin}(k) = max(P_{fcs,min}, P_{el}(k) - P_{b,max}) \tag{3.31}$$

$$P_{fcs,Ymax}(k) = min(P_{fcs,max}, P_{el}(k) - P_{b,min}) \tag{3.32}$$

It is important to note that minimum battery power $P_{bat,min}$ is defined as a negative value. All constraints used in the cost function are documented in Table 2.1.
In comparison to $\boldsymbol{Y_{ref}}$, the values for $P_{fcs,Ymin}$ and $P_{fcs,Ymax}$ are calculated at each sampling instance due to the changing demand of electrical power.

## 3.3 Processing of predictive information

### Averaging of predicted electric power

The processing of predicted power demand needs to be adapted. Firstly, due to the new concept for the MPC, the number of rows of $\boldsymbol{\Delta U}$ and $\boldsymbol{\Delta Z}$ are reduced by removing zero values. Furthermore, the disturbance signal is assumed to act simultaneously with the control signal. Secondly, a forecast of $P_{el}$ over the entire prediction horizon Np is never accurate due to various assumptions and disturbances (e.g., velocity assumption, driver's behaviour). Therefore, the prediction is averaged between the computational points of the disturbance variables. In Figure 3.3, the basic idea of this approach is depicted.

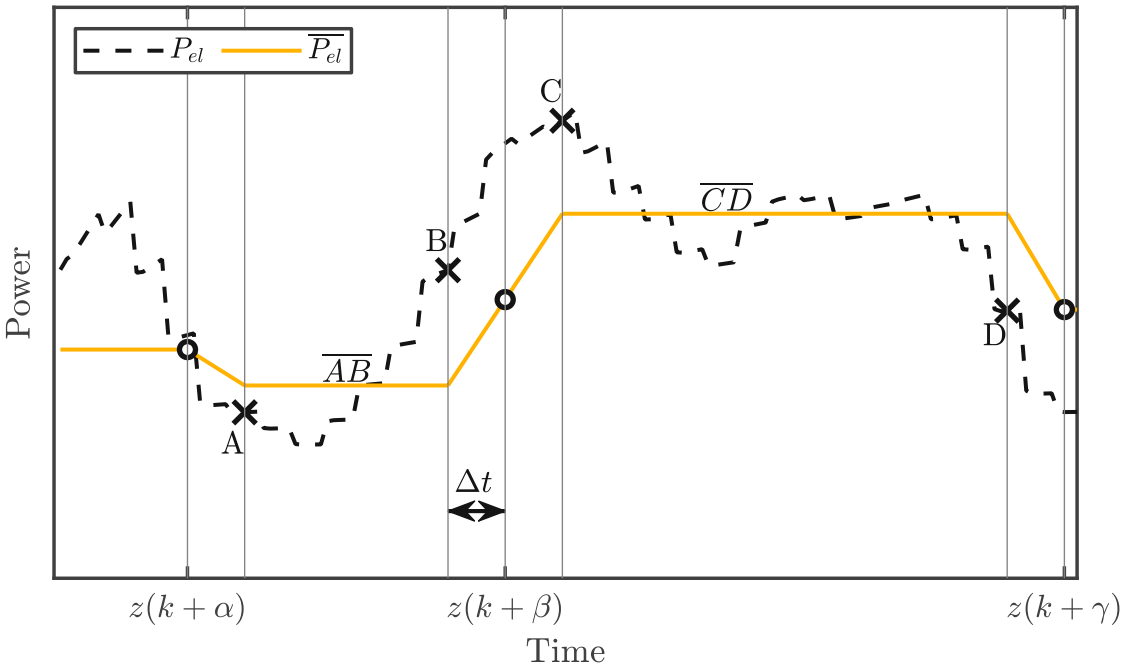


Figure 3.3: Averaging of predicted electric power.

In this example, points A and C are each one time step after a disturbance variable and B and D one time step before. First of all, the values $\overline{AB}$ and $\overline{CD}$ are calculated by using the arithmetic mean. Then it is possible to compute the desired disturbance value $z(k+\beta)$ by averaging $\overline{AB}$ and $\overline{CD}$. With this approach, a coherent $\overline{P_{el}}$ can be achieved that still depicts the original prediction.

## Control variables distributed over the horizon

In Figure 3.4 two different methods to calculate the distribution between the control variables, are depicted. For this representation the prediction horizon is 900 seconds and the number of control variables is 10. The first control variable is always at time step one and the next variable acts for a uniformly distribution at $t = 1 + \Delta$ and for a non-uniformly distribution $t = 1 + \Delta_1$. The third variable acts at $t = 1 + \Delta + \Delta$ and $t = 1 + \Delta_1 + \Delta_2$, respectively, and so forth.

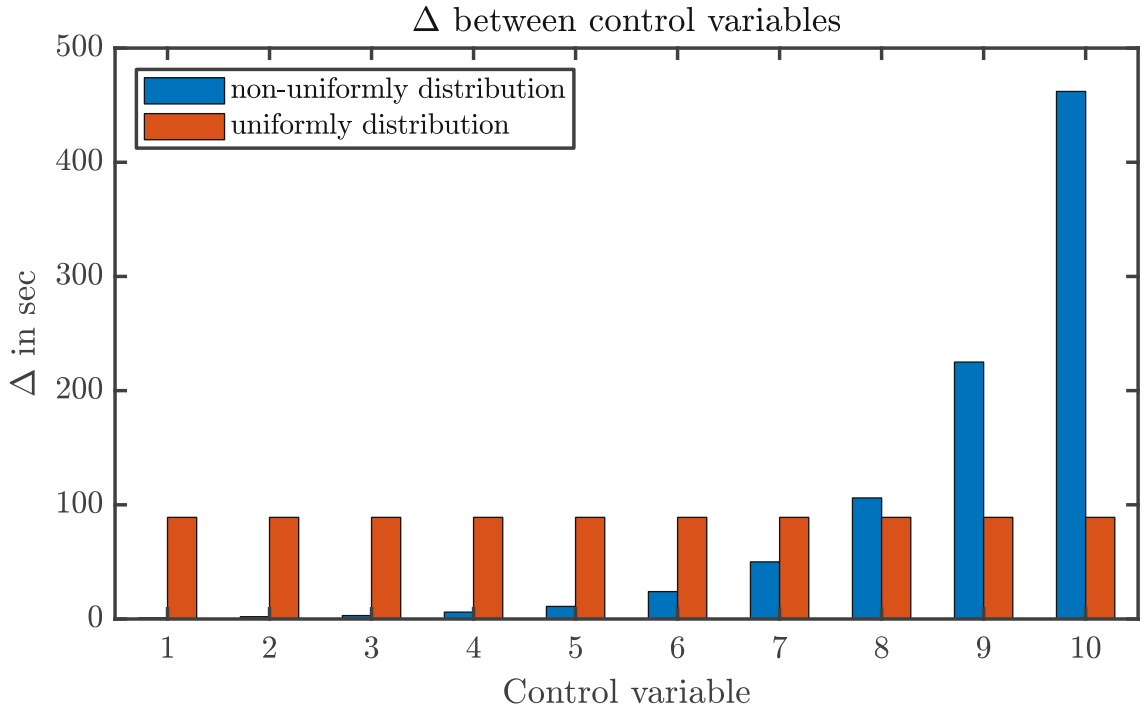


Figure 3.4: Comparison between two distribution methods.

In Figure 3.5 and Figure 3.6 two cases for the averaging of predicted electric power are presented. If the non-uniformly distribution method is used, then there will be a high distribution of control variables in the near future. This can potentially lead to better predictions of the future state variables. Since there is also one control variable in the middle of the prediction horizon, in this case at $t = 438s$, the trend of the electric power is included in the calculation.
Compared to the non-uniformly distribution, uniformly distributed control variables $\overline{P_{el}}$ better reflect the trend of the function $P_{el}$. Therefore, both approaches are analysed and compared in this thesis.

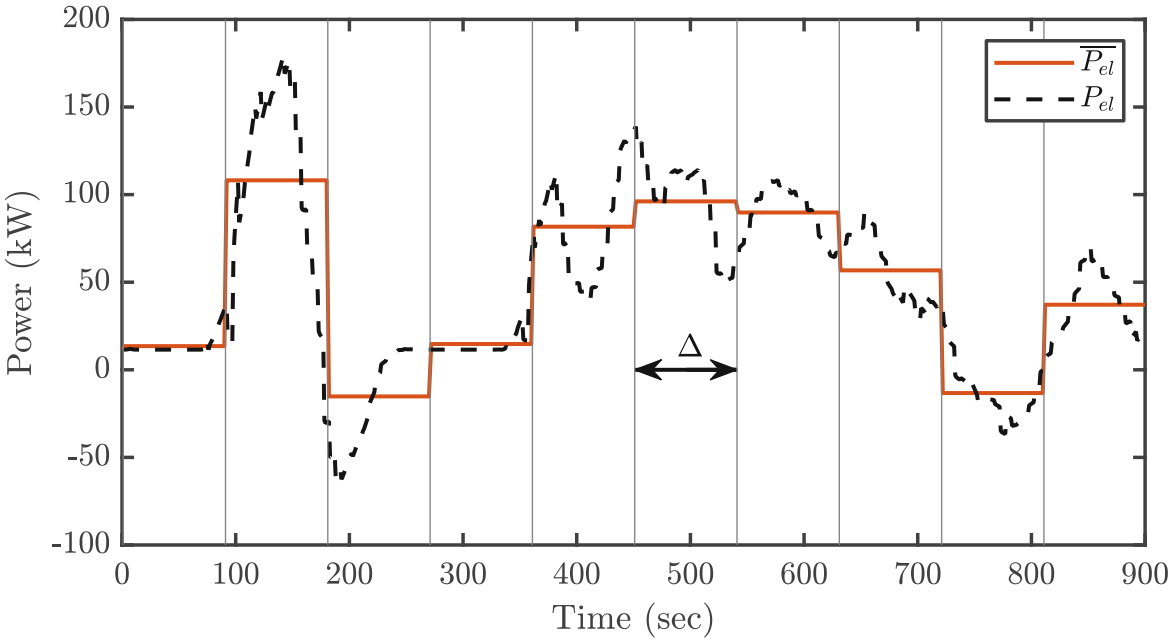


Figure 3.5: Averaged electric power, uniformly distributed control variables.

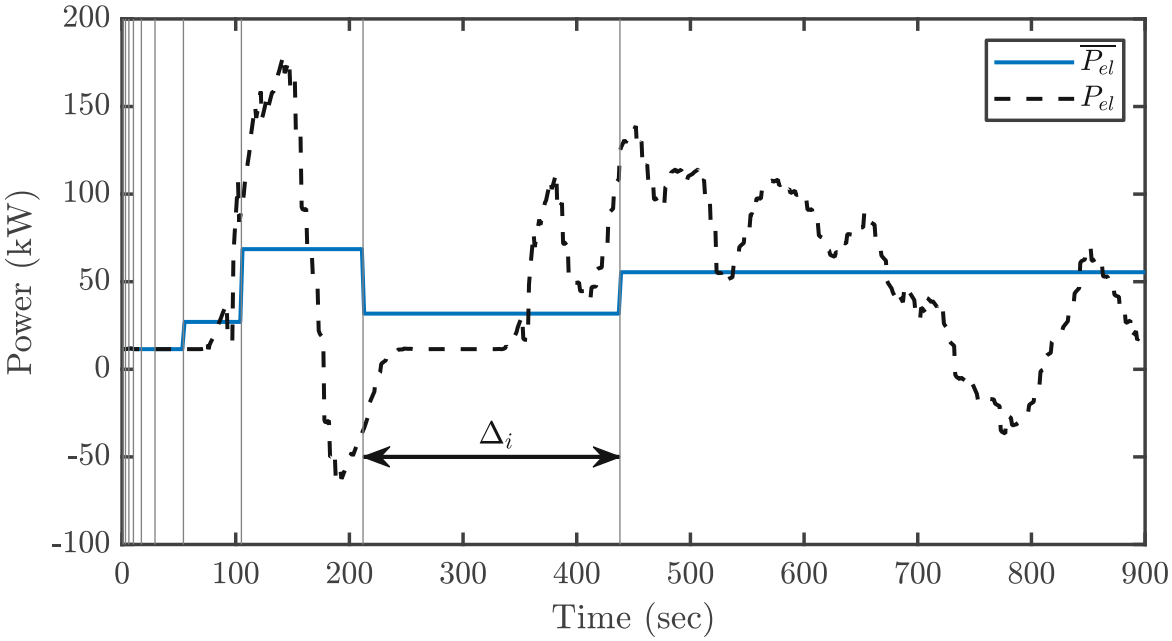


Figure 3.6: Averaged electric power, non-uniformly distributed control variables.

## Prediction of the required electric power

Based on the road information, a predictive energy management system uses the longitudinal model to calculate the required electric power for the driving cycle. (see in Figure 2.5). An accurate prediction of the required power is essential for the PEMS to minimise objective functions. Therefore, future driving conditions are one of the primary prediction objectives in the literature. The future driving condition can be obtained using telemetry devices or environment detecting sensors like global positioning systems (GPS) and radars [20].
Due to the ubiquitous access to real-time data, a PEMS can enhance the performance of the vehicle by including short-term information like distribution of traffic signals, traffic congestion level, or unexpected movements of preceding vehicles [20].
For this thesis, two driving cycles are considered, and both consist of an elevation and a velocity profile. The road slope has a high impact on the electrical loads due to the increased mass of the heavy-duty vehicle. It is assumed that the elevation profile is known at each time step.
Predicting the velocity is a challenging task. Therefore, simplified prediction methods are proposed. For example, the simplest assumption for a velocity profile is a constant velocity. However, this can be problematic because the predicted electrical power is too high or low during acceleration or deceleration phases.
An alternative approach is a speed limit assumption. This case has the benefit that it is more likely to be closer to the actual driving behaviour than a constant velocity assumption, but it still varies from the actual velocity.
However, one could use recorded data of the driving cycle for the velocity profile. Using such a profile can lead to an incorrect forecast due to different drivers' behaviours or uncertainties of real-world driving conditions.
Consequently, vehicle speeds and accelerations cannot be accurately predicted. For simplicity, constant velocity and speed limits with a known elevation profile are used for the prediction of the required power. Four cases are proposed to adjust the predicted electrical power with respect to the input desired by the driver. However, any velocity assumption can be used for the long-term prediction of the required electric power.

### Offline calculation of the demanded power

In Figure 3.7 case 1 is depicted. Before the simulation, the predicted electric power $P_{el}$ is calculated with a speed assumption and an elevation profile. During the simulation, the predicted electric power is modified: at time step t=k, the desired value by the driver is used, and the remaining prediction remains unchanged.

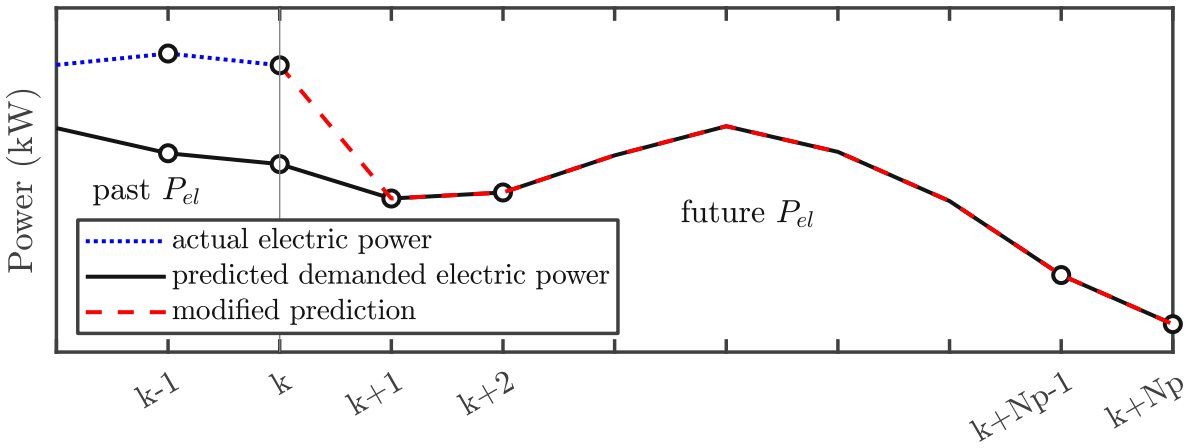


Figure 3.7: Case 1.

Case 2 is identical to case 1, except that the transition between the desired value and the prediction is realised with a sigmoid function. This allows for a smooth transition (see Figure 3.8).

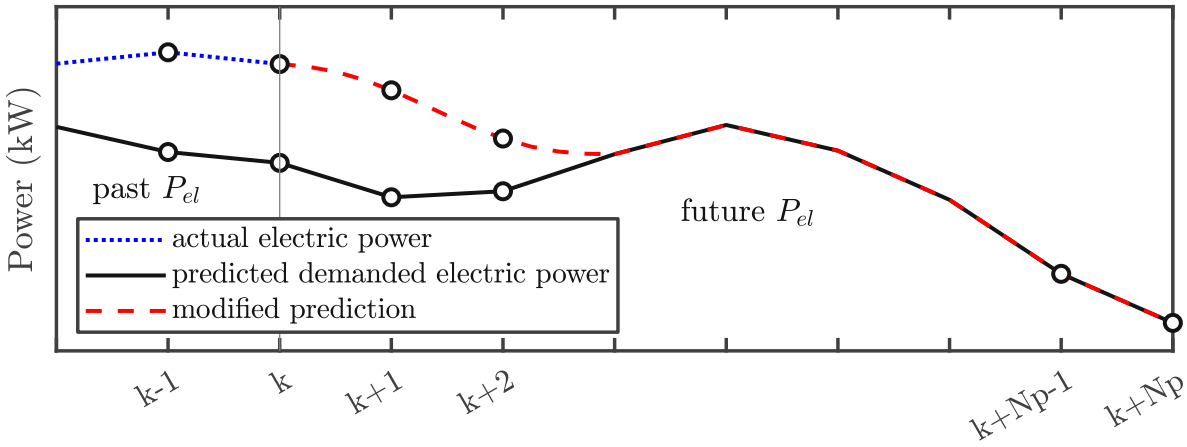


Figure 3.8: Case 2.

## Online calculation of the demanded power

The calculation of the demanded power is based on a constant modification of the velocity assumption (see Figure 3.9). A sigmoid function is used during the simulation for the transition between the actual velocity and the velocity assumption. The required electric power is predicted at each step using the elevation profile.

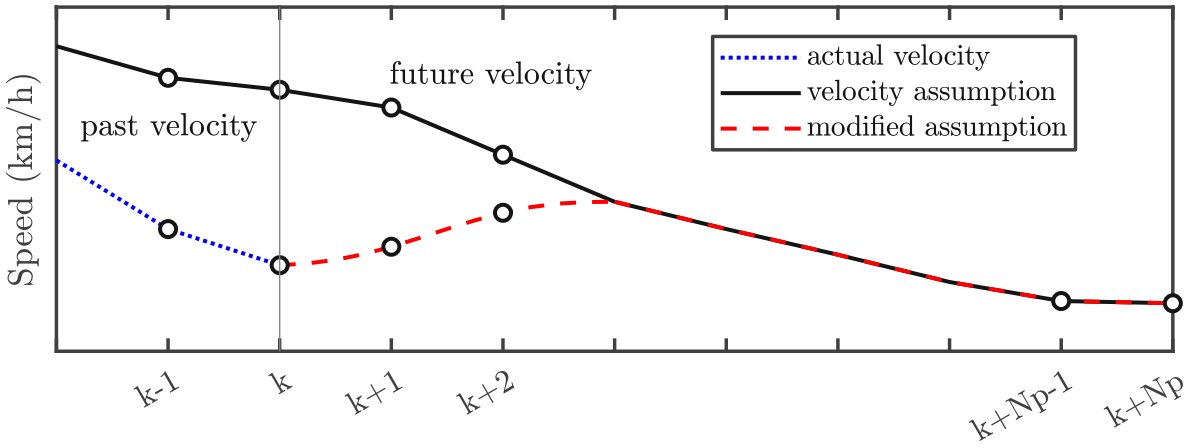


Figure 3.9: Case 3.

In Figure 3.10 it can be seen that case 4 is unique. No velocity assumption is needed for this case because the predicted velocity is calculated by averaging the past measured velocity. Also, a sigmoid function is used for the transition between the actual velocity and the velocity profile assumption. The required electric power is predicted based on the velocity and elevation profiles.

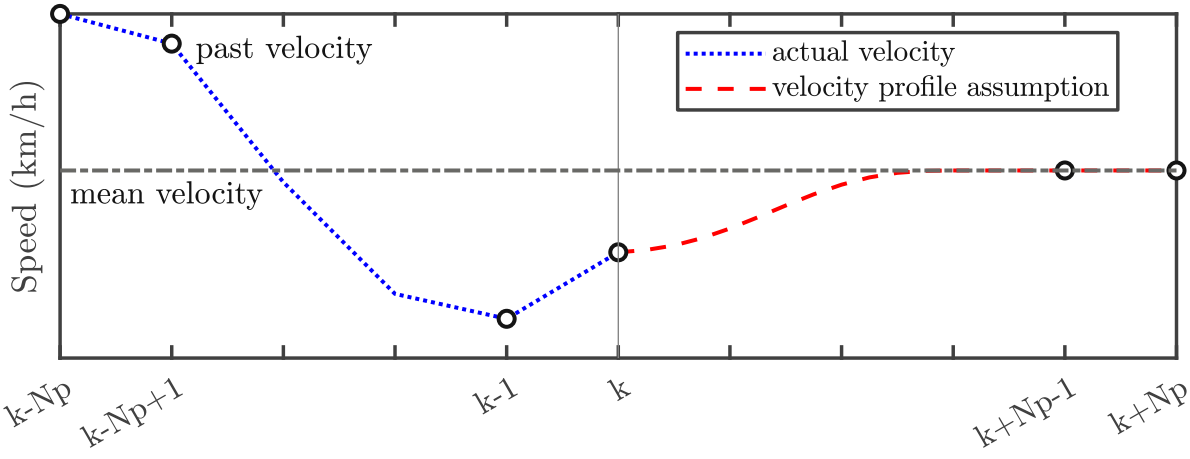


Figure 3.10: Case 4.

## 3.4 Implementation in MATLAB/ SIMULINK

In Figure 3.11 the scheme of implementation in *SIMULINK* is depicted. The vehicle model block, which consists of the longitudinal model, the fuel cell system and the battery model, receives the velocity $v$ and the elevation profile $h$ from the driving cycle. The electric power demand is predicted based on the elevation profile and velocity estimation. Depending on which prediction case is chosen, $P_{el,est}$ is calculated either before or during simulation. The MPC is embedded into a Level-2 MATLAB S-Function, because this custom block handles multiple input and output ports [21]. The MPC has the current distance *s(k)*, velocity *v(k)*, acceleration *a(k)*, the desired electric power $P_{des}(k)$, the state of energy *SoE(k)* and the estimated electric power demand $P_{el,est}$ as an input.

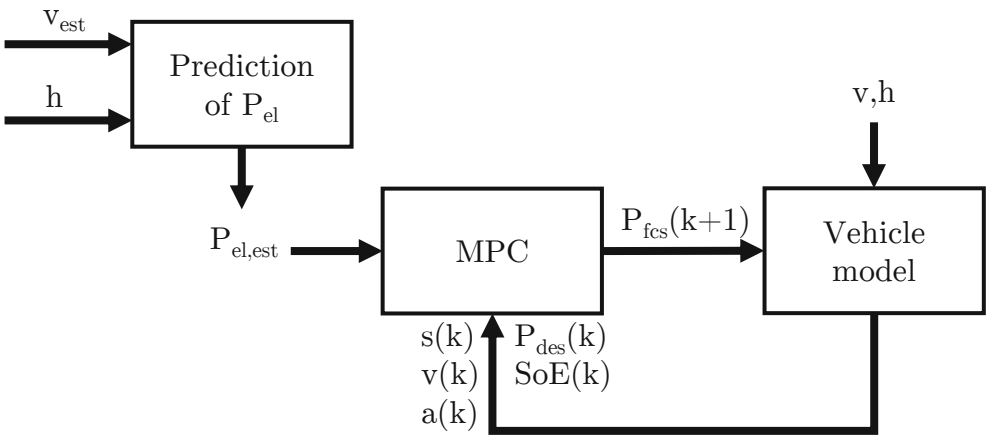


Figure 3.11: Scheme of implementation in *SIMULINK*.

With all the input, the cost function is solved with *qpOASES*, which is an open-source implementation to solve quadratic programs [22]. The output of the model predictive controller is the optimal fuel cell power for the next time step $P_{fcs}(k+1)$.
In addition to the *SIMULINK* blocks, *MATLAB* functions are called before the simulation to calculate the augmented matrices for the MPC and to load necessary parameters for the simulation. In *section A.1* a listing of all *MATLAB* functions and their descriptions are documented.

# Chapter 4

# Simulation results

In this chapter, the proposed predictive energy management system is tested and validated. For the simulation, real-world driving data of heavy-duty vehicles for road freight transportation are considered.
The influence of the prediction horizon and the number and distribution of control variables on hydrogen consumption and simulation time are examined. Afterwards, the robustness of the MPC is investigated.

## 4.1 Simulation framework

All the simulations are performed using MATLAB R2021b. SIMULINK uses an ode1(Euler) solver with a fixed-step size of $\Delta t = 0.2$s and the model predictive controller has a sampling time of 1s.
Information on the driving cycles are provided in Table 4.1. In Figure 4.1 and Figure 4.2 the speed, elevation and the electrical power demand profile of both driving cycles is shown.

Table 4.1: Driving cycle characteristics

| | Average speed | Total distance | Driving time |
|---|---|---|---|
| Driving cycle A | 72 km/h | 316 km | 262 min |
| Driving cycle B | 69 km/h | 385 km | 333 min |

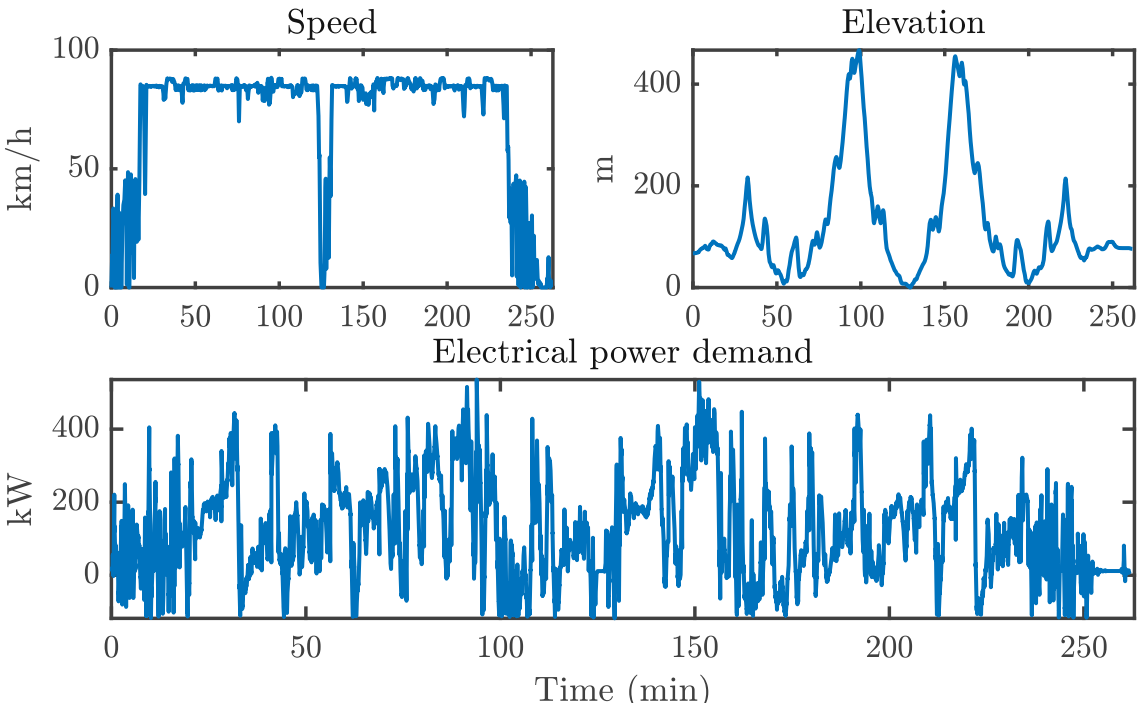


Figure 4.1: Driving cycle A: speed, elevation, electrical power demand.

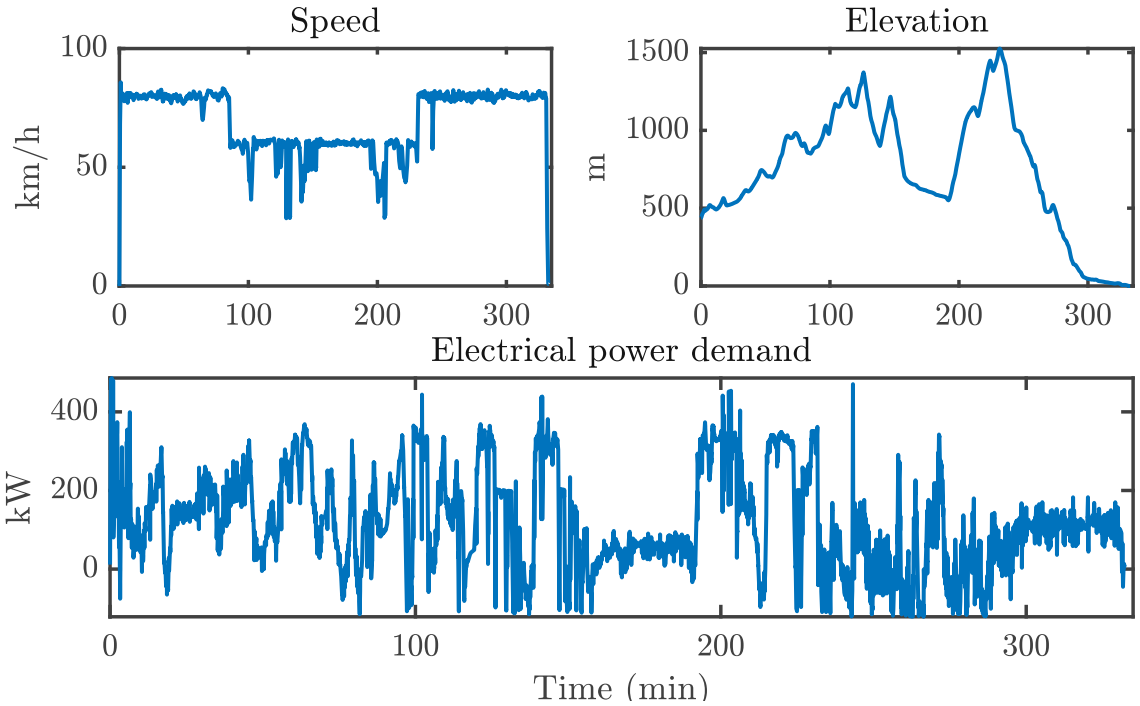


Figure 4.2: Driving cycle B: speed, elevation, electrical power demand.

The calculation of fuel consumption $m_{H2,fcs}$ is straightforward, it depends on the fuel cell power $P_{fcs}$, the efficiency of the fuel cell $\eta_{fcs}$ and the hydrogen lower heating value LHV.

$$m_{H2,fcs} = \int \frac{P_{fcs}}{LHV \cdot \eta_{fcs}} dt \tag{4.1}$$

One goal of the MPC is SoE control, but there is no constraint for the final SoE value. The final SoE value can be higher or lower than the reference for some MPC configurations. Therefore, an equivalent H2 consumption is introduced to account for the short-term use of the fuel cell at the end of the simulation: $m_{H2,bat}$ depends on the initial and final value of SoE, the nominal battery energy $E_{b,nom}$, the average efficiency of the fuel cell $\eta_{fcs,avg}$ and the hydrogen lower heating value LHV.

$$m_{H2,b} = \frac{(SoE_I - SoE_F) \cdot E_{b,nom}}{LHV \cdot \eta_{fcs,avg}} \tag{4.2}$$

With both equations the adapted hydrogen consumption is calculated in the following way:

$$m_{H2} = m_{H2,fcs} + m_{H2,b} \tag{4.3}$$

Furthermore, it is necessary to specify cases 2,3 and 4 because they all depend on a sigmoid function. For the three cases, three different methods are used to calculate the duration length of the sigmoid function. It is a constant value for case 2, and for case 3 and case 4, the value depends on the prediction horizon. This approach is chosen because due to the similarities of the cases, using different methods can verify the robustness of the MPC. For this thesis, the defined methods are fixed and are not examined further, although modifying them will affect the results. In Table 4.2 the values are documented.

Table 4.2: Sigmoid function - duration length

| | case | length (seconds) |
|---|---|---|
| Online calculation of $P_{el}$ | 1 | not needed |
| | 2 | 45 |
| Offline calculation of $P_{el}$ | 3 | $0.05 \times Np$ |
| | 4 | $0.6 \times Np$ |

The weight matrices **Q** and **R** from the cost function had to be carefully chosen to achieve comparability between the prediction horizons. The known required electrical power is plugged into case 1, and the weight matrices are tuned to yield a similar SoE function for four different prediction horizons (see Figure 4.3(a)). In Figure 4.3(b) the decreasing hydrogen consumption with increasing prediction horizon is depicted.

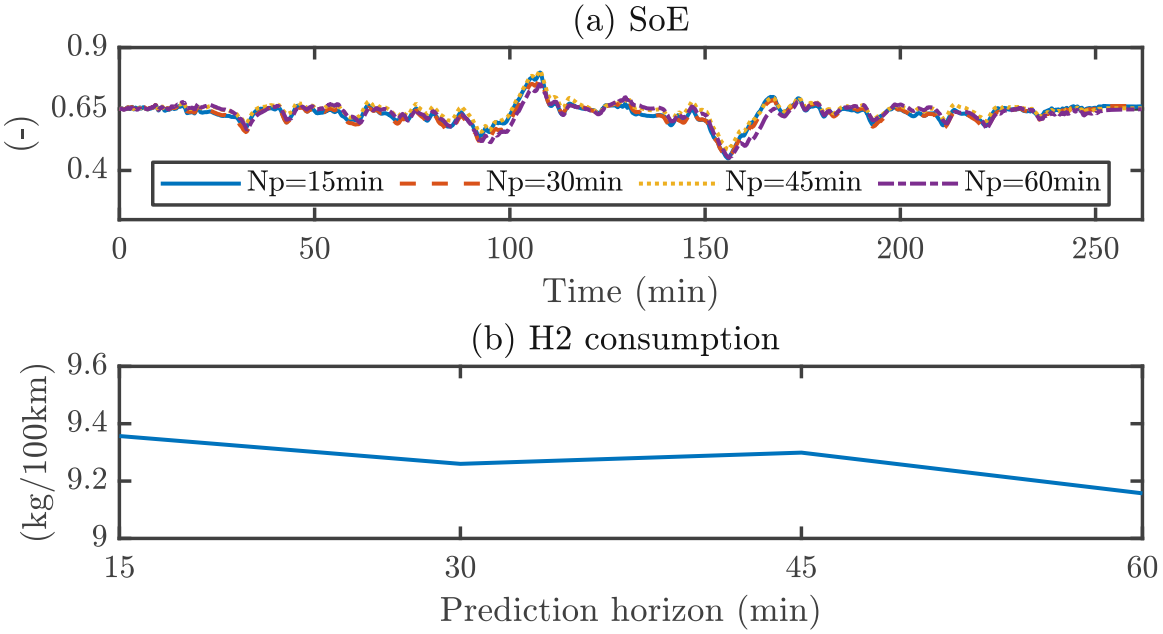


Figure 4.3: Comparison of four different prediction: (a) SoE, (b) H2 consumption.

The weight matrices are documented in Table 4.3. A different configuration of the weight matrices is required for each prediction horizon. For example, as the prediction horizon increases, the value for **Q(1)** decreases. A lower value means that the MPC tries less to minimise the margin of error between the predicted state of energy and the reference value.

Table 4.3: Weight matrices

| Np (min) | Q | R | $R_{slack}$ |
|---|---|---|---|
| 15min | $[3e^2 \quad 1e^{-10}]$ | $1e^{-9}$ | $1e^3$ |
| 30min | $[1e^2 \quad 1e^{-10}]$ | $4e^{-9}$ | $1e^4$ |
| 45min | $[1e^2 \quad 1e^{-10}]$ | $1e^{-8}$ | $1e^3$ |
| 60min | $[9e^1 \quad 1e^{-10}]$ | $1e^{-7}$ | $1e^3$ |

## 4.2 Analysis on model predictive control parametrization

In this section, several parameters are varied to examine the behaviour of the model predictive control. The prediction of the demanded electric power is based on a constant velocity assumption of v=72 km/h, and driving cycle A is considered for the simulation.

### Analysis on prediction horizon and number of control variables

The first analysis examines the influence of the number of control variables and the length of the prediction horizon on hydrogen consumption and computational complexity. The results for the simulation time are shown in Figure 4.4.

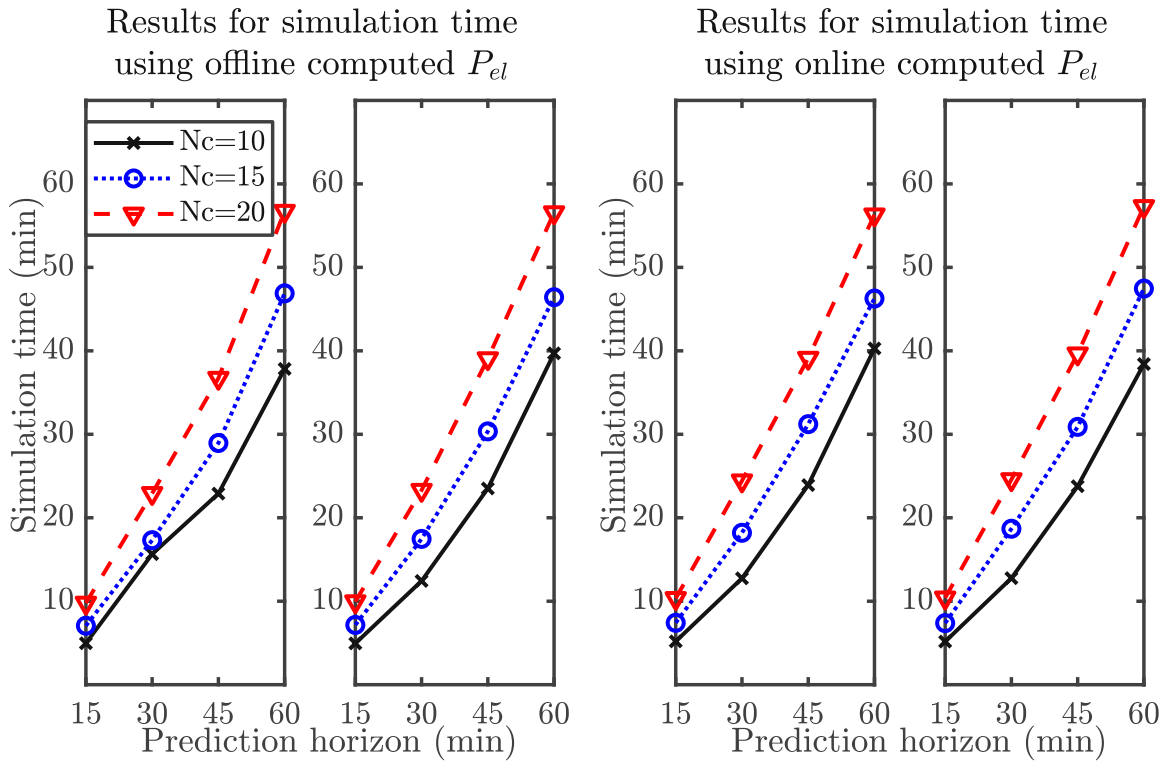


(a) Case 1 (left), case 2 (right)

(b) Case 3 (left), case 4 (right)

Figure 4.4: Simulation time depending on the number of control variables and length of prediction horizon.

Predicting the required electric power before the simulation (case 1 and case 2) does not decrease simulation time compared with online computing the necessary electric power (case 3 and case 4). Since, in case 1, the prediction is not modified with a sigmoid function, the simulation time is slightly lower compared to the other cases.
A high prediction horizon and a higher number of decision variables lead to a significantly higher simulation time (see Figure 4.4). This results from the fact that *qpOASES* needs more time to find the optimal $\boldsymbol{\Delta U}$ to minimise the cost function due to larger matrices. A four times larger prediction horizon leads to six to eight times longer simulation time.

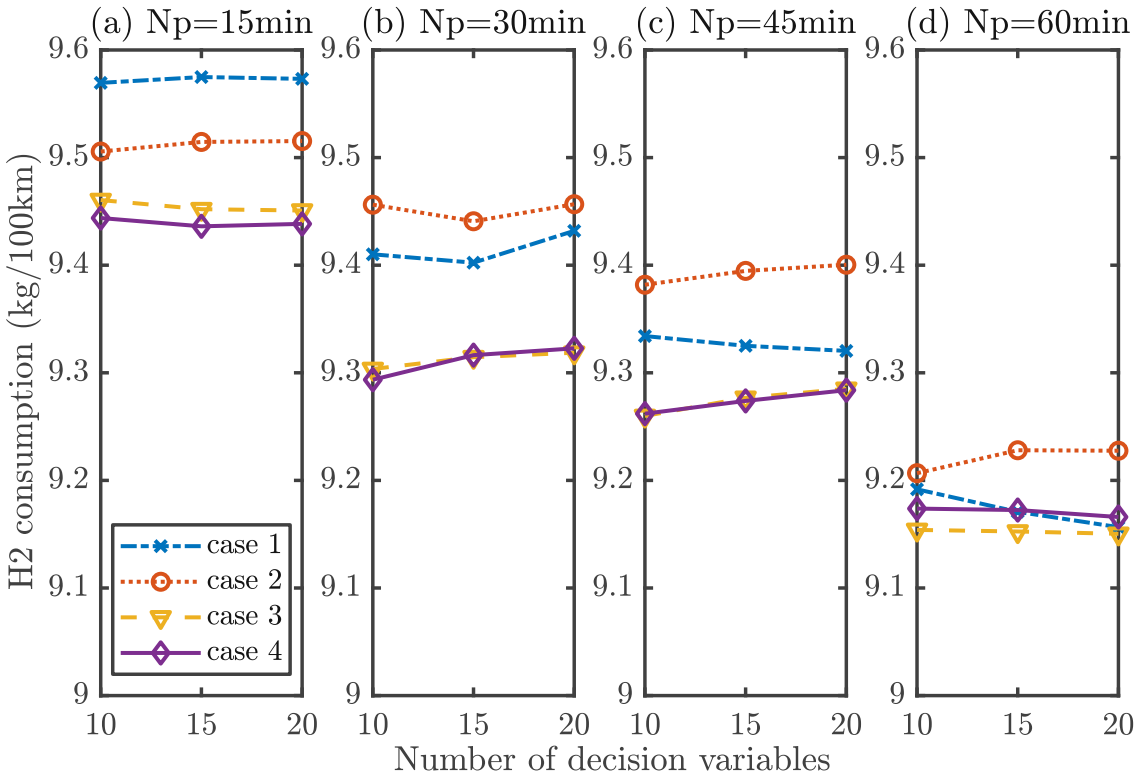


Figure 4.5: H2 consumption depending on the number of decision variables and length of prediction horizon.

In Figure 4.5 the hydrogen consumption for the driving cycle A is presented. It can be easily seen that a higher prediction horizon leads to fewer hydrogen consumption of the vehicle. This result is expected because the MPC has more information on the driving cycle with a higher prediction horizon at each time step. This allows the vehicle to drive with more foresight and take better account of uphill and downhill sections, leading to better results. Although the hydrogen consumption decreases with increasing prediction

horizon, regardless of the number of decision variables, it is not evident whether a higher number of decision variables leads to fewer hydrogen consumption. For $Np = 45\text{min}$, a higher number of control variables reduce the hydrogen consumption for case 1, while for the other three cases the hydrogen consumption increases (see Figure 4.5(c)).

## Interpretation of the results

The different behaviour of hydrogen consumption is investigated for a prediction horizon of 45min. Case 1 and case 2 are considered, differing only by the sigmoid function used in case 2. In both cases, the same velocity assumption is used to predict the electrical power before the simulation. In Figure 4.6, it is shown that for case 1 with an increasing number of control variables, the regenerative energy increases, while the fuel cell energy decreases. For case 2, it is exactly the opposite (see (a) and (b)). To neglect the influence of the final SoE value, the results for the hydrogen consumption $m_{H2,fcs}$, which only depend on the fuel cell power, the efficiency of the fuel cell and the hydrogen lower heating value are presented in Figure 4.6(c). In case 1, the consumption decreases, while in case 2, it increases. Therefore, the difference in behaviour results from the sigmoid function used in case 2.

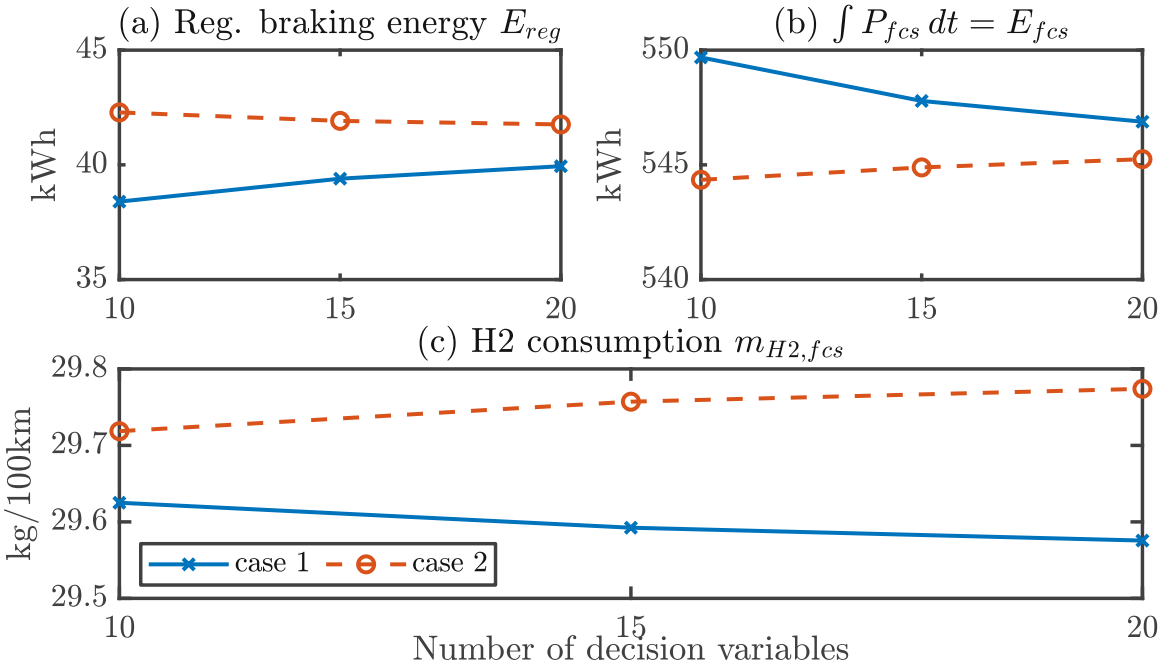


Figure 4.6: Comparison between case 1 and case 2.

## Analysis on the distribution of control variables

An assumption, based on Figure 3.6, is, that an uniformly distribution of decision variables better reflect the trend of the function $P_{el}$. This could lead to better results. Therefore, a simulation is performed with ten decision variables, a constant velocity assumption of 72km/h on the driving cycle A with different distribution methods.
In Figure 4.7 the results for the simulation time depending on distribution of decision variables for different prediction horizon is shown. For case 1 and Np=30min, and for case 4 and Np=60min, there is a noticeable difference between the results. Otherwise, unlike the number of variables, the distribution of the decision variables has no significant influence on the simulation time.

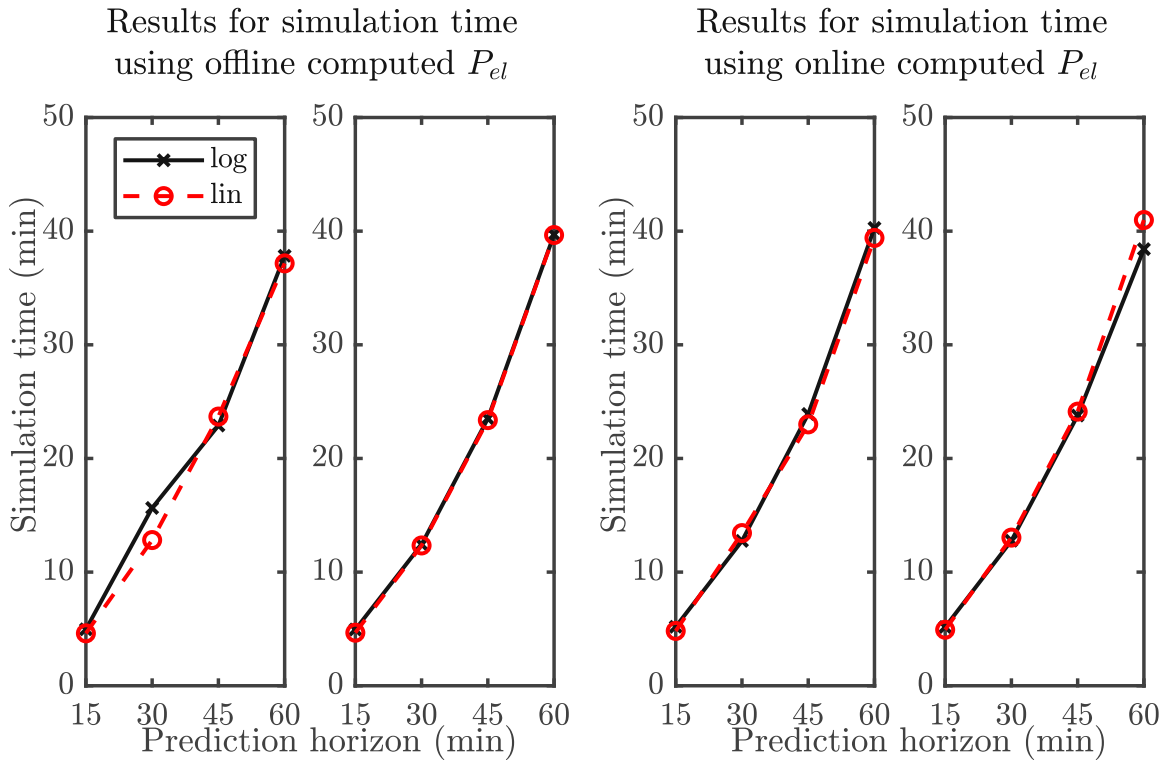


(a) Case 1 (left), case 2 (right)

(b) Case 3 (left), case 4 (right)

Figure 4.7: Simulation time depending on distribution of decision variables - log = non-uniform distribution, lin = uniform distribution.

Although the distribution method does not affect computational complexity, it has an impact on the hydrogen consumption (see Figure 4.8). In contrast to the non-uniformly distribution, the uniform distribution does not decrease values for hydrogen consumption as the prediction horizon increases.

A higher prediction horizon allows the MPC to have more foresight of the driving cycle. Still, with a uniform distribution, MPC optimises for moments in time that are too far away in the future and are not relevant for the next step.

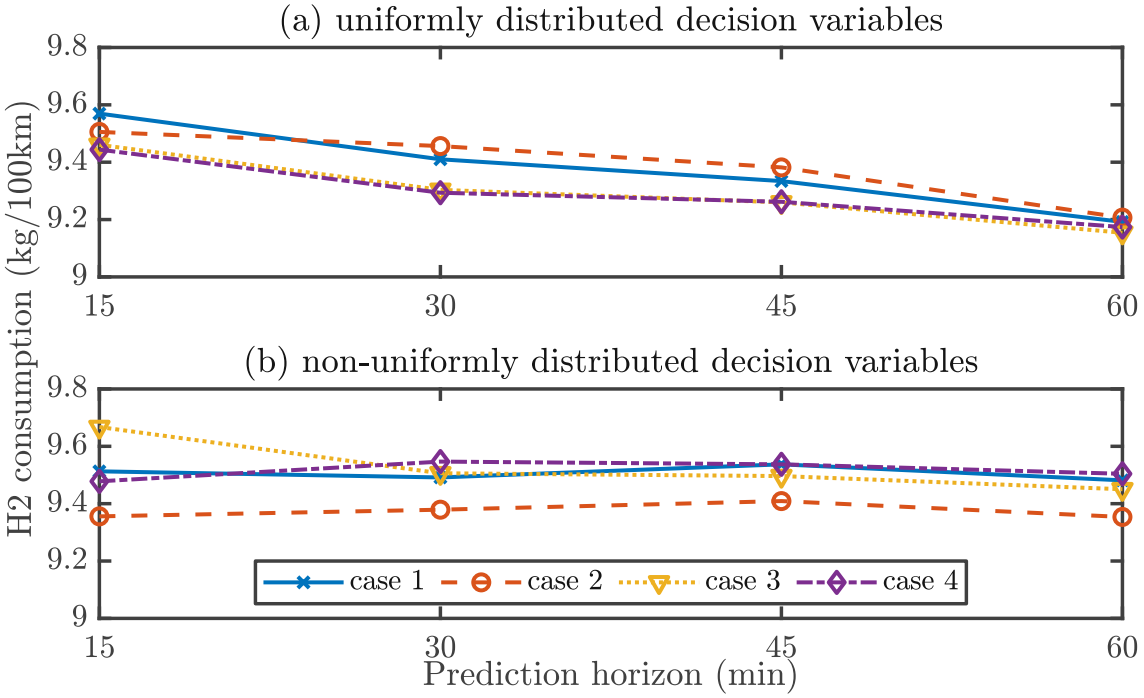


Figure 4.8: H2 consumption depending on the number of decision variables.

The influence of the distribution method can also be seen in Figure 4.9. For case 1, the regenerative braking and the fuel cell energy results are compared. With uniformly distributed decision variables, regenerative braking decreases while the used fuel cell energy increases, resulting in higher hydrogen consumption.

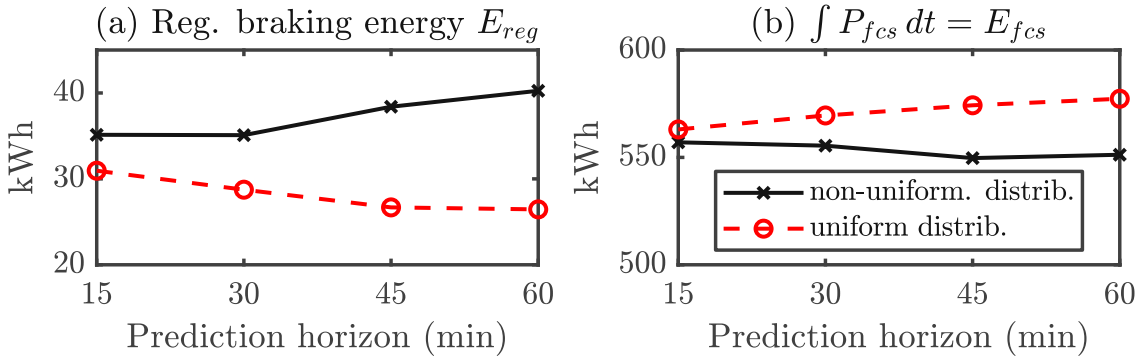


Figure 4.9: Comparison of regenerated energy and fuel cell energy - case 1.

## 4.3 Validation on robustness

Validation of the results is necessary, first, to verify that the MPC provides useful predictions and, second, that the predictive energy management strategy is correctly implemented in *SIMULINK*.
In general, it must be verified if the energy management system meets the driver's requirements. First of all, the difference between the actual velocity and the velocity desired by the driver should be small:

$$\epsilon_v = v - v_{des} < 1\text{m/s} \tag{4.4}$$

Also, one input of the MPC is the electric power $P_{el,des}$ desired by the driver. The minimum value for the fuel cell power, which is required to achieve the desired value by the driver, is calculated by reformulating (3.14) using the maximum battery constraint:

$$P_{fcs,min,des} = P_{el,des} - P_{b,max} \tag{4.5}$$

The fuel cell power calculated by the MPC should always be equal to or greater than $P_{fcs,min,des}$.
The last validation requirement is the exitflag from *qpOASES*. After every calculation *qpOASES* returns a simple status flag [22]. The status flag indicates if the quadratic problem is solved, infeasible or unbounded. Therefore, this must be checked to guarantee a robust energy management system.
For further analysis, the parameters for the model predictive control are fixed (see Table 4.4).

Table 4.4: Overview of the simulation parameters

| | |
|---|---|
| Prediction horizon (Np) | 15min, 30min, 45min, 60min |
| Number of control variables (Nc) | 10 |
| Distribution method | non-uniformly |
| Velocity assumptions for driving cycle A | v=72km/h & v=speed limit |
| Velocity assumptions for driving cycle B | v=69km/h & v=speed limit |

## Checking the robustness

To analyse the robustness of the MPC, it is investigated whether the validation parameters are violated. In Table 4.5, the robustness check is documented for the two cases where the required electrical power is calculated offline. It can be easily seen that qpOASES has no problems solving the quadratic problem and that the margin of error $\epsilon_v$ between the actual velocity and the desired speed is low enough. In addition, the optimal fuel cell power provided by the MPC is high enough to achieve the electrical power required by the driver.

Table 4.5: Offline calculation of $P_{el}$ (case1, case2): overview of robustness check - driving cycle A & B

| Velocity assumption | qpOASES | $\epsilon_v$ | $P_{fcs,min,des}$ |
|---|---|---|---|
| v = const | Pass | Pass | Pass |
| v = speed limit | Pass | Pass | Pass |

In Table 4.6 the results are documented for the two cases where the required electrical power is calculated online. The minimum fuel cell power requirement is violated for both speed assumptions.
The violation of the condition is attributed to the definition of case 3 and case 4. For case 3, a sigmoid function is used for a smooth transition between the desired velocity and the velocity assumption. Afterwards, the required electric power is predicted. The duration of the "S"-shaped curve of the sigmoid function can significantly change the result prediction. In case 4, the predicted velocity is calculated by averaging the past measured velocity. Therefore, neither the desired velocity nor the desired fuel cell power are considered. A solution to avoid constraint violation for both cases is to modify the original definition. In both cases, it must be checked if the online calculated electrical power is greater than the electrical power desired by the driver.

Table 4.6: Online calculation of $P_{el}$ (case3, case4): overview of robustness check - driving cycle A & B

| Velocity assumption | qpOASES | $\epsilon_v$ | $P_{fcs,min,des}$ |
|---|---|---|---|
| v = const | Pass | Pass | Failed |
| v = speed limit | Pass | Pass | Failed |

## Analysis of hydrogen consumption

Since the online calculation of $P_{el}$ violates the minimum fuel cell power requirement, case 3 and case 4 are not examined further. Only case 1 will be investigated further since the only difference from case 2 is the sigmoid function, and the use of this function does not significantly affect hydrogen consumption.
In Figure 4.10 the hydrogen consumption for driving cycle A and B with different velocity assumptions is depicted. It can be seen that a higher prediction horizon does not lead to fewer hydrogen consumption for driving cycle B.

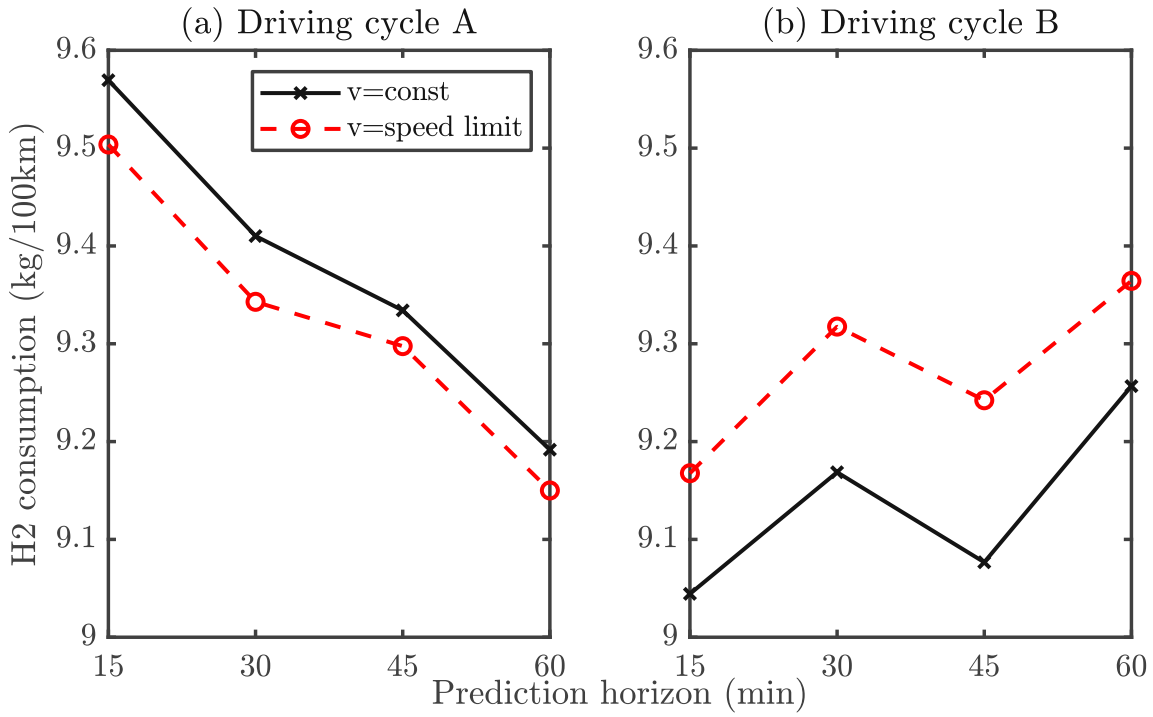


Figure 4.10: Comparison of hydrogen consumption - case 1.

A speed limit assumption is closer to the actual velocity than a constant velocity assumption. Therefore, the prediction of the required electrical power is more accurate, resulting in lower hydrogen consumption. This is the case for driving cycle A, but not for driving cycle B.
Due to the cost function, the MPC tries to minimise the error between the reference value $SoE_{ref}$ and the predicted $SoE(k+1)$ value. This leads to the assumption that the weight matrices are an essential factor in the different behaviour of the MPC between the two driving cycles.

## Modification of the weight matrices of the cost function

The matrices are changed to check whether they are responsible for the contrasting results in Figure 4.10. The changes concern mainly the matrix **R**. The values for **R** are increased, and by doing so, the input signal, $P_{fcs}$, is used less by the MPC.
The comparison between the old and new weight matrices is documented in Table 4.7.

Table 4.7: Comparison of the weight matrices

| Np (min) | $Q_{new}$ | $R_{new}$ | $R_{slack,new}$ | Q | R | $R_{slack}$ |
|---|---|---|---|---|---|---|
| 15min | $[3e^2 \quad 1e^{-10}]$ | $1e^{-8}$ | $1e^3$ | $[3e^2 \quad 1e^{-10}]$ | $1e^{-9}$ | $1e^3$ |
| 30min | $[3e^2 \quad 1e^{-10}]$ | $4e^{-7}$ | $1e^3$ | $[1e^2 \quad 1e^{-10}]$ | $4e^{-9}$ | $1e^4$ |
| 45min | $[1e^2 \quad 1e^{-10}]$ | $3e^{-7}$ | $1e^3$ | $[1e^2 \quad 1e^{-10}]$ | $1e^{-8}$ | $1e^3$ |
| 60min | $[1e^2 \quad 1e^{-10}]$ | $4e^{-7}$ | $1e^3$ | $[9e^1 \quad 1e^{-10}]$ | $1e^{-7}$ | $1e^3$ |

Different results for the driving cycle A and B are obtained by modifying the weight matrices. In Figure 4.11 the hydrogen consumption for driving cycle A and driving cycle B with a speed limit assumption and ten decision variables is presented. It can be seen in (a) that the results computed with the modified weight matrices are lower than for results calculated with the original weight matrices. For driving cycle B, the results are lower, and with a higher prediction horizon, the hydrogen consumption decreases.
Due to the changes in the weight matrix, the MPC is distributing less of the demanded electric load to the fuel cell. The battery has to provide more energy so that the MPC can meet the required power.
Since the result for SoE is the same for all four prediction horizons, only the prediction horizon of Np=45min is presented in Figure 4.12. The lower values for hydrogen consumption are a result of higher utilisation of the battery, which in turn violates the soft constraint $SoE_{min} = 0.4$. With a different drive cycle, the changed weight matrices could lead to a complete battery discharge. This could reduce battery life or violate the driver's desired acceleration input.

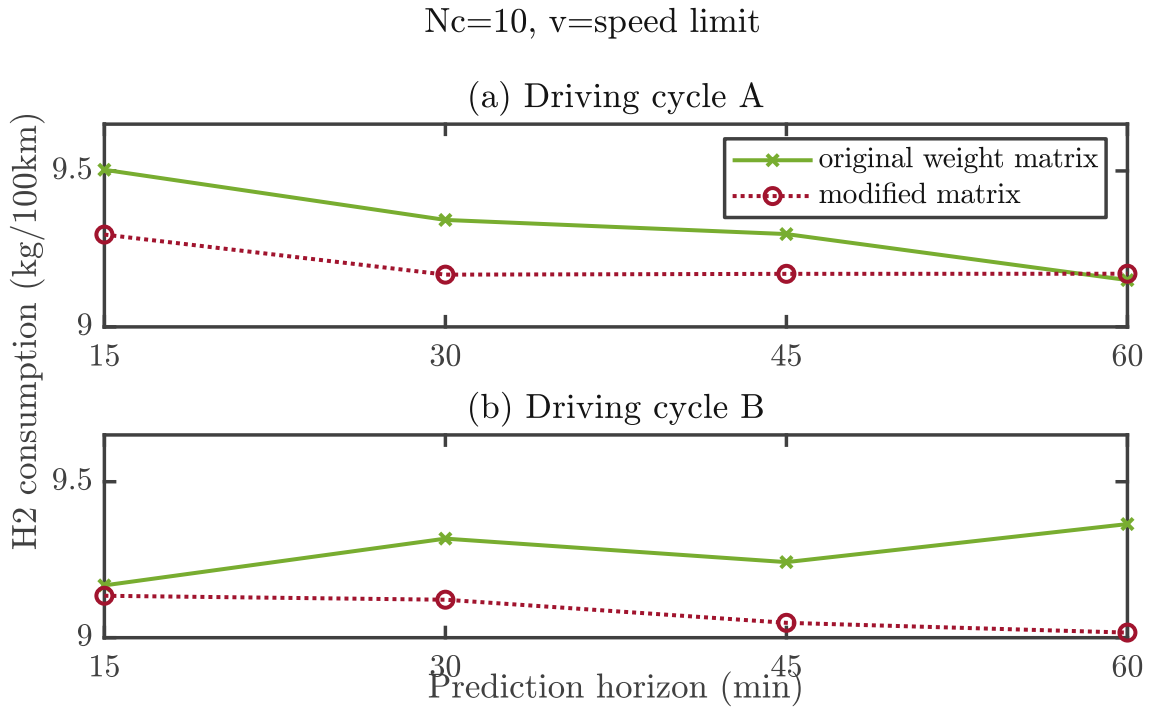


Figure 4.11: H2 consumption for (a) driving cyle A, (b) driving cycle B.

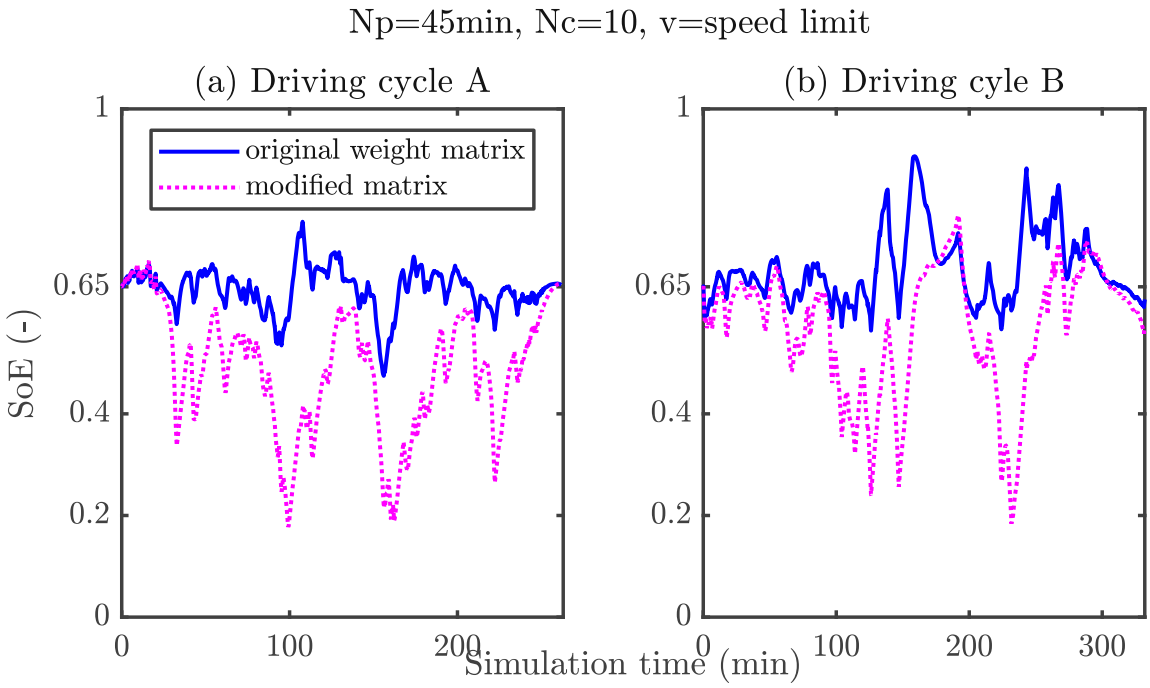


Figure 4.12: SoE for (a) driving cyle A, (b) driving cycle B.

# Chapter 5

# Conclusion

This thesis proposes a novel method for a predictive energy management strategy based on model prediction control. After modifying the basic mathematical definition to design a predictive controls system, the energy management system is then embedded into a suitable simulation framework.
The influence of the prediction horizon and the number and distribution of control variables on hydrogen consumption and simulation time are examined.
One investigation result is that the simulation time increases significantly with an increasing prediction horizon. A four times larger prediction horizon can lead to six to eight times longer simulation time. In contrast, hydrogen consumption decreases with an increasing prediction horizon. A higher number of control variables increases the simulation time, but it does not necessarily reduce the hydrogen consumption. Furthermore, the research shows that a high density of control variables in the near future leads to better results in terms of hydrogen consumption than a uniform distribution over the entire prediction horizon.
The investigations are conducted with two methods for predicting the required electric power: the demanded power is calculated before or during the simulation. The main knowledge gained from this approach is that the MPC has to incorporate the electric power desired by the driver for a robust energy management strategy. If this is not guaranteed, the optimal fuel cell power results are suboptimal.
The energy management strategy includes only the state of energy control and fuel cell power utilisation. This is a potential research direction as battery and fuel cell lifetime could be incorporated into the strategy.
This thesis illustrates that the proposed predictive energy management system works in principle. Still, it raises the question of whether it is possible to implement the controller in online energy management of heavy-duty fuel cell electric vehicles. Therefore, further investigations are needed to answer whether such an implementation can be done.

Further investigations to evaluate the robustness of the PEMS are required. Not only should additional driving cycles be considered, but also disturbances and uncertainties caused by driver behaviour or traffic conditions impact the stability and robustness of the proposed controller.
Overall, more research is needed to guarantee that the MPC can find an optimal solution without violating any constraints. In addition, another online energy management strategy should be used to generate benchmark values to compare the results from the MPC against.

# Appendix A

# Appendix

## A.1 Listing of MATLAB Functions

### Functions

| File | Description |
|---|---|
| Run.m | Main file. The main parameters for the simulation are defined in here. |
| load_param.m | This is called in Run.m. It uses the parameters from the main file to calculate the necessary matrices for the calculation during the simulation. |
| generate_nc_sequence.m | Function. With the main parameters this file creates a vector that indicates the distribution of the actuating variables |
| mpc_matrices.m | Function. This file creates the matrices for the MPC |
| mean_of_p_fcs_calculation.m | Function. It calculates the average of the predicted power. |
| MPC_EMS_Sfunction.m | Level-2 MATLAB S-function. Main file for the MPC. It loads the desired case and it uses qpOASES to solve the quadratic problem. |

# Bibliography


[1] European Environment Agency (EEA). New registrations of electric vehicles in europe. https://www.eea.europa.eu/ims/new-registrations-of-electric-vehicles, 2021. URL `https://www.eea.europa.eu/ims/new-registrations-of-electric-vehicles`. Accessed: 2022-02-08.

[2] Seemungal L, Arrigoni A, Davies J, Weidner Ronnefeld E, and Hodson P. Decarbonisation of heavy duty vehicle transport: Zero emission heavy goods vehicles. -, 1(KJ-NA-30773-EN-N (online)), 2021. ISSN 1831-9424 (online). doi: 10.2760/790827(online).

[3] Huan Li, Alexandre Ravey, Abdoul N'Diaye, and Abdesslem Djerdir. A review of energy management strategy for fuel cell hybrid electric vehicle. In *2017 IEEE Vehicle Power and Propulsion Conference (VPPC)*, pages 1–6, 2017. doi: 10.1109/VPPC.2017.8330970.

[4] Farzad Rajaei Salmasi. Control strategies for hybrid electric vehicles: Evolution, classification, comparison, and future trends. *IEEE Transactions on Vehicular Technology*, 56(5):2393–2404, 2007. doi: 10.1109/TVT.2007.899933.

[5] Antonio Sciarretta Lino Guzzella. *Vehicle Propulsion Systems*. Springer, Berlin, Heidelberg, 2013. ISBN 9783642359125. doi: 10.1007/978-3-642-35913-2.

[6] Pei Zhang, Fuwu Yan, and Changqing Du. A comprehensive analysis of energy management strategies for hybrid electric vehicles based on bibliometrics. *Renewable and Sustainable Energy Reviews*, 48:88–104, 2015. ISSN 1364-0321. doi: https://doi.org/10.1016/j.rser.2015.03.093. URL `https://www.sciencedirect.com/science/article/pii/S1364032115002464`.

[7] Chao Sun, Scott Jason Moura, Xiaosong Hu, J. Karl Hedrick, and Fengchun Sun. Dynamic traffic feedback data enabled energy management in plug-in hybrid electric vehicles. *IEEE Transactions on Control Systems Technology*, 23(3):1075–1086, 2015. doi: 10.1109/TCST.2014.2361294.

[8] Hansang Lim, Wencong Su, and Chunting Chris Mi. Distance-based ecological driving scheme using a two-stage hierarchy for long-term optimization and short-term adaptation. *IEEE Transactions on Vehicular Technology*, 66(3):1940–1949, 2017. doi: 10.1109/TVT.2016.2574643.

[9] Saeid Zendegan, Alessandro Ferrara, Stefan Jakubek, and Christoph Hametner. Predictive battery state of charge reference generation using basic route information for optimal energy management of heavy-duty fuel cell vehicles. *IEEE Transactions on Vehicular Technology*, 70(12):12517–12528, 2021. doi: 10.1109/TVT.2021.3121129.

[10] Guotao Xie, Hongbo Gao, Lijun Qian, Bin Huang, Keqiang Li, and Jianqiang Wang. Vehicle trajectory prediction by integrating physics- and maneuver-based approaches using interactive multiple models. *IEEE Transactions on Industrial Electronics*, 65(7):5999–6008, 2018. doi: 10.1109/TIE.2017.2782236.

[11] Oleg Gomozov, João Pedro F. Trovão, Xavier Kestelyn, and Maxime R. Dubois. Adaptive energy management system based on a real-time model predictive control with nonuniform sampling time for multiple energy storage electric vehicle. *IEEE Transactions on Vehicular Technology*, 66(7):5520–5530, 2017. doi: 10.1109/TVT.2016.2638912.

[12] G Mohan, F Assadian, and S Longo. Comparative analysis of forward-facing models vs backwardfacing models in powertrain component sizing. In *IET Hybrid and Electric Vehicles Conference 2013 (HEVC 2013)*, pages 1–6, 2013. doi: 10.1049/cp.2013.1920.

[13] M. Kandidayeni, A. Macias, A.A. Amamou, L. Boulon, S. Kelouwani, and H. Chaoui. Overview and benchmark analysis of fuel cell parameters estimation for energy management purposes. *Journal of Power Sources*, 380:92–104, 2018. ISSN 0378-7753. doi: https://doi.org/10.1016/j.jpowsour.2018.01.075. URL `https://www.sciencedirect.com/science/article/pii/S0378775318300752`.

[14] Alessandro Ferrara, Michael Okoli, Stefan Jakubek, and Christoph Hametner. Energy management of heavy-duty fuel cell electric vehicles: Model predictive control for fuel consumption and lifetime optimization. *IFAC-PapersOnLine*, 53 (2):14205–14210, 2020. ISSN 2405-8963. doi: https://doi.org/10.1016/j.ifacol.2020.12.1053. URL `https://www.sciencedirect.com/science/article/pii/S2405896320314233`. 21st IFAC World Congress.

[15] Alessandro Ferrara, Stefan Jakubek, and Christoph Hametner. Energy management of heavy-duty fuel cell vehicles in real-world driving scenarios: Robust design of strategies to maximize the hydrogen economy and system lifetime. *Energy Conversion and Management*, 232:113795, 2021. ISSN 0196-8904. doi: https://doi.org/10.1016/j.enconman.2020.113795. URL https://www.sciencedirect.com/science/article/pii/S0196890420313182.

[16] Arash Shafiei, Ahmadreza Momeni, and Sheldon S. Williamson. Battery modeling approaches and management techniques for plug-in hybrid electric vehicles. In *2011 IEEE Vehicle Power and Propulsion Conference*, pages 1–5, 2011. doi: 10.1109/VPPC.2011.6043191.

[17] Abbas Fotouhi, Daniel J. Auger, Karsten Propp, Stefano Longo, and Mark Wild. A review on electric vehicle battery modelling: From lithium-ion toward lithium–sulphur. *Renewable and Sustainable Energy Reviews*, 56:1008–1021, 2016. ISSN 1364-0321. doi: https://doi.org/10.1016/j.rser.2015.12.009. URL https://www.sciencedirect.com/science/article/pii/S1364032115013921.

[18] Gaizka Saldaña, José Ignacio San Martín, Inmaculada Zamora, Francisco Javier Asensio, and Oier Oñederra. Analysis of the current electric battery models for electric vehicle simulation. *Energies*, 12(14), 2019. ISSN 1996-1073. doi: 10.3390/en12142750. URL https://www.mdpi.com/1996-1073/12/14/2750.

[19] Liuping Wang. *Model Predictive Control System Design and Implementation Using MATLAB*. Springer Publishing Company, Incorporated, 1st edition, 2009. ISBN 1848823304.

[20] Yang Zhou, Alexandre Ravey, and Marie-Cécile Péra. A survey on driving prediction techniques for predictive energy management of plug-in hybrid electric vehicles. *Journal of Power Sources*, 412:480 – 495, 2019. URL https://hal.archives-ouvertes.fr/hal-02130788.

[21] MATLAB. *version 9.11.0.1769968 (R2021b)*. The MathWorks Inc., Natick, Massachusetts, 2022.

[22] et al Ferreau, H.J. *qpOASES User's Manual*. https://github.com/coin-or/qpOASES. URL https://github.com/coin-or/qpOASES.